MOMENTUM AND HEAT TRANSFER STUDIES

I. Transfer of Heat and Momentum in Uniform
    Turbulent Air Streams

II. Continuous Velocity Measurements by the
    Hot Wire Method

Thesis by

Robert Mitchell Sherwin

In Partial Fulfillment of the Requirements

for the degree of

Chemical Engineer

California Institute of Technology

Pasadena, California

1952

ACKNOWLEDGMENT

This thesis is dedicated to those who have worked on the transfer research program. May their experiences and contributions be appreciated by future students, whose enthusiasm will grow as they become increasingly familiar with the program which Dr. B. H. Sage is directing.

The writer is grateful to W. G. Schlinger for his guidance and to H. H. Reamer for his useful suggestions. Special thanks are due to Evelyn Anderson, who typed the manuscript, and to Virginia Berry, who prepared the figures.

ABSTRACT

Part I

The thermal flux has been measured across an air stream flowing in a uniform, two-dimensional manner between horizontal parallel plates at different temperatures. Reynolds numbers ranged from 9,800 to 56,500. A macroscopic correlation shows the effect of turbulence on the thermal transfer.

A revised correlation of total conductivity as a function of position is subsequently obtained by correcting previously determined values of total conductivity. A similar correlation of the total viscosity with position is revised to allow for variation in the pressure gradient with plate separation. The correlations fall off with increasing Reynolds number. The turbulent Prandtl numbers for two tests by an earlier investigator are compared with those predicted from the ratio of the revised point correlations.

Part II

Two hot-wire methods are described for determining continuously the mean velocity as a function of position in a turbulently-flowing air stream. In the constant-resistance method the mean wire temperature is automatically controlled. In the constant-current method no control is necessary. In exploratory measurements the total viscosities bridge the discontinuous gap which arises from the use of von Kármán's expression at the boundary between the buffer layer and the turbulent core. Thermal flux corresponding to a Nusselt number of 40 has no noticeable effect on the velocity profile.

TABLE OF CONTENTS

Part I

Introduction:

In 1874 Osborne Reynolds (1) suggested the proportionality between velocity and temperature profiles in a turbulently flowing fluid near a heat-exchanging surface, thereby laying groundwork for the boundary layer theories of L. Prandtl (2) and G. I. Taylor (3). The modified boundary layer theory of von Kármán (4) includes the concept of a turbulent core surrounded by a buffer zone, which is enclosed by a laminar layer at the wall. The presence of velocity and temperature gradients indicates the transfer of momentum and thermal energy. The transfer in the core takes place as the result of macroscopic eddy motion. In the laminar layer the transfer occurs by the interaction of molecules. The buffer layer is a transition between the core and the laminar layer.

One of the objectives of the transfer research program of the Chemical Engineering Department of the California Institute of Technology has been to explore the relationship between the transfer of heat and the transfer of momentum. The role of the eddy quantities is of immediate interest. For the case of two-dimensional uniform flow these quantities may be defined as follows:

$$\epsilon_m = \underline{\epsilon}_m - \nu = \frac{T}{\rho} \frac{1}{\frac{\partial u}{\partial y}} - \nu \tag{1}$$

$$\epsilon_c = \underline{\epsilon}_c - K = \frac{\overset{\circ}{Q}}{C_p \sigma} \frac{1}{\frac{\partial t}{\partial y}} - K \tag{2}$$

where ϵ_m is the portion of total viscosity attributed to turbulence, ν is the portion of total viscosity attributed to molecular agitation, τ is the shear, ρ is the density, and $\frac{\partial u}{\partial y}$ is the velocity gradient normal to the flow of the stream. In the second equation ϵ_c is the portion of total conductivity attributed to turbulence, K is the portion attributed to molecular agitation, $\overset{\circ}{Q}$ is the heat flux across the stream, C_p is the specific heat, σ is the specific weight, and $\frac{\partial t}{\partial y}$ is the temperature gradient across the stream. $\underline{\epsilon}_m$ and $\underline{\epsilon}_c$ are the total viscosity (5) and the total conductivity, respectively. ν and K are the common molecular properties of viscosity, η , and conductivity, k , reduced to common dimensional units by the following equations:

$$\nu = \frac{\eta}{\rho} \qquad (3)$$

$$K = \frac{k}{C_p \sigma} \qquad (4)$$

For flow between parallel plates τ is obtained from the relationship:

$$\tau = \left(\frac{y_0}{2} - y_d \right) \frac{dP}{dx} \qquad 5)$$

where $\frac{dP}{dx}$ is the pressure gradient, $\frac{y_0}{2}$ is the distance from the wall to the point of maximum velocity, and y_d is the distance from the wall to the point in question.

In Equation (2) the relationship between the eddy quantity and the gradient is somewhat different from that of Equation (1). $\overset{\circ}{Q}$ is constant across the stream, whereas $\mathcal{T}$ varies linearly with position. From the standpoint of the boundary layer theory, however, the eddy viscosity, ϵ_m, and the eddy conductivity, ϵ_c, are zero at any point in the laminar layer. They increase gradually in the buffer region and make a sudden jump as the point moves into the turbulent core. If it is assumed that momentum and heat are transferred by the same physical process a simple analysis (6) shows that:

$$\underline{\epsilon}_m = \underline{\epsilon}_c \tag{6}$$

For fluids in which $\dfrac{\nu}{K}$, the Prandtl number, equals 1:

$$\nu = K \tag{7}$$

Therefore:

$$\underline{\epsilon}_m - \nu = \underline{\epsilon}_c - K$$
$$\text{or} \qquad \epsilon_m = \epsilon_c \tag{8}$$

The common gases have Prandtl numbers which are approximately unity.*

- - - - - - - - - -

* For diatomic gases at one atmosphere and 212° F., $\dfrac{\nu}{K} = 0.74$ (7)

If the total viscosity and the total conductivity are equal, then:

$$\epsilon_c = \epsilon_m = \epsilon = \frac{\tau}{\rho} \frac{1}{\frac{\partial u}{\partial y}} \tag{9}$$

Because τ and $\frac{\partial u}{\partial y}$ both go to zero at the point of maximum velocity, the relationship appears indeterminate. If the von Kármán universal velocity distribution were applicable, then:

$$\begin{aligned} u+ = \frac{u}{u*} &= 5.5 + 5.75 \log y+ \qquad (y+ > 30)\\ &= 5.5 + 5.75 \log \frac{y_d u*}{\nu} \end{aligned} \tag{10}$$

where u is the mean point velocity in the direction of flow and $u*$ is defined by the equation:

$$u* = \sqrt{\frac{\tau_o}{\rho}} \tag{11}$$

τ_o being the shear at the wall. From Equation (10) $\frac{\partial u}{\partial y}$ is always finite. Hence ϵ should go to zero at the center. Recent experimental work, however, indicates that the total eddy quantities are not equal and do not approach zero at the center (8). These results indicate that the Reynolds analogy is not exact, and it is an accepted fact that the von Kármán distribution law diverges from universality at the center. It is therefore a matter of interest to measure the eddy quantities independently and thereby examine the extent to which the Reynolds analogy holds.

The material reported in this thesis is an extension of
the work carried on by S. D. Cavers, who succeeded in showing a
limited correlation between the total viscosity, the total conduc-
tivity, and position in the stream (6). Such a correlation differs
from the overall relationships commonly used in transfer problems
in that it establishes a path through the transfer medium. The
film concept, widely used in chemical engineering calculations,
deliberately avoids consideration of this path.

From the known macroscopic correlations between Reynolds
number, Prandtl number, and Nusselt number (9) the possibility is
suggested that similar correlations may exist at a geographical
point in a flowing stream. Various dimensionless functions have
been suggested as representing the degree of turbulence at a point,
or the local Reynolds number. One of these, already used in
Equation (10), is the friction-distance parameter $y+$ (10)[*]:

$$ y+ \ = \ \frac{y_d \, \mu^*}{\nu} \tag{12} $$

----

[*] Another parameter, the stability factor χ, is mentioned by
Rouse (11), where:

$$ \chi = y_d^{\,2} \frac{\partial \mu}{\partial y} \frac{1}{\nu} $$

By the appropriate substitutions for the case of symmetrical flow
it may be shown that this is identical with the expression:

$$ \chi = y+^2 \left(\frac{1 - \frac{2y_d}{y_o}}{\frac{\epsilon_m}{\nu}} \right) = \frac{y+^2}{\theta} $$

For the von Kármán velocity distribution:

$$ \theta = \frac{y+}{2.5} $$

in the turbulent core. Hence:

$$ \chi = 2.5 \, y+ $$

and the two quantities χ and $y+$ are proportional in the core.

The local turbulent Prandtl number at a point may be defined as:

$$\frac{\epsilon_m}{\epsilon_c} = Pr'$$
(13)

The local Nusselt number loses significance[*]:

$$\lim \frac{\mathring{Q}}{\Delta t} \frac{\Delta y}{\epsilon_c} = \frac{\mathring{Q}}{\epsilon_c} \frac{1}{\frac{\partial t}{\partial y}} = Nu' = 1$$
(14)

Thus the following relationship is suggested:

$$Nu' = f_1 (Re')(Pr')$$
(15)

which can be reduced to:

$$\frac{\epsilon_c}{\epsilon_m} = f_2 (y+)$$
(16)

An expression similar to Equation (16) may be arrived at in connection with flow between parallel plates. Starting with the von Kármán universal velocity distribution equation:

$$u+ = f_3 (y+)$$
(17)

- - - - - - - - - -

[*] The interpretation of Nusselt number here is open to debate. Martinelli (7) shows that the macroscopic Nusselt number is merely the ratio of the temperature gradient at the boundary to the average temperature gradient across the conduit. von Kármán describes the local Nusselt number as $\frac{\epsilon_c}{\kappa}$, or the multiple of conduction transferred by convection. In Equation (14) conduction is implicitly redefined to include convection. Hence the ratio is unity.

and assuming that maximum velocity occurs half way between the plates, Cavers showed that:

$$\frac{\epsilon_m}{\nu}\left(\frac{1}{1-\frac{2y_d}{y_o}}\right) = \frac{1}{f_3'(y+)} = f_4(y+) \qquad (18)$$

where y_o is the plate separation. The equation for total conductivity from the standpoint of the Reynolds analogy would be:

$$\frac{\epsilon_c}{K}\left(\frac{1}{1-\frac{2y_d}{y_o}}\right) = f_5(y+) \qquad (19)$$

Dividing (19) by (18):

$$\frac{\epsilon_c}{\epsilon_m}\frac{\nu}{K} = \frac{f_5(y+)}{f_4(y+)} = f_6(y+) \qquad (20)$$

Equation (20) differs from Equation (16) by a factor of $\frac{\nu}{K}$, the molecular Prandtl number. This variable was not considered in the steps leading up to Equation (13). As the ratio of molecular momentum transfer to molecular heat transfer, however, the Prandtl number may be readily envisaged as a variable affecting both boundary and point conditions.

Description of the Equipment:

The apparatus used to study the Reynolds analogy has been described by Billman (12) and Corcoran (13) and is discussed here briefly for convenience. Two $\frac{1}{4}$ inch by 12 inch by $13\frac{1}{2}$ foot long copper plates are mounted horizontally with a separation of 0.7 inch. Air is made to flow longitudinally in the space between the plates,

which are sealed off by blocks at the sides to form a closed tunnel
(Figures 1, 2, and 3). Because of the large aspect ratio* of the
resulting channel the conditions approach those of ideal two-
dimensional flow between parallel plates. The plates are held at
different controlled temperatures by means of circulating oil baths,
and the air is supplied by a variable-speed centrifugal blower.

A traversing gear with probe, Figure 4, permits the measure-
ment of point temperatures and velocities by the thermanemometer
method (12). Shear quantities may be calculated from pressure gra-
dients measured by piezometer bars in the upper plate and by static
taps in the side blocks.

The two calorimeters are those described by Cavers (6),
being vacuum-jacketed, shielded blocks flush with the lower side of
the upper plate, (Figure 5). Each is independently supplied with
electrical energy so as to be at the same temperature as the surround-
ing plate. The thermal flux is obtained by measuring the rate of
addition of electrical energy. The calorimeters are located $6\frac{1}{2}$ feet
and 11 feet downstream from the air entrance.

The air enters the channel at a temperature half way be-
tween the plate temperatures. In passing down the channel it is
brought to a state where its static, kinetic, and thermodynamic
properties do not appreciably change along the flow axis. Thus at
the working section there is no component of energy transferred from
the plates in the axial direction. Such conditions are desirable for
a study of the Reynolds analogy inasmuch as the transfer of momentum
also takes place normal to the direction of flow.

- - - - - - - - -

* Defined as the ratio of width to depth

Experimental Methods:

A complete set of calorimetric measurements was made in the same general manner described by Cavers (6). The Reynolds numbers varied from 9,800 to 56,500. In all tests the upper plate was maintained at the higher temperature so that gravitational convective effects could be neglected, and cooling fluid was not required for the calorimeters. The effects of jacket-vacuum, room temperature, and plate losses were also estimated as before. To minimize the losses further the circulating oil to each calorimeter jacket was heated to maintain it at the upper plate temperature, and the upper extremities of the wire leads from the calorimeters were heated to the nominal upper plate temperature.

Conduction losses to the upper plate and losses to the room were carefully measured at several different temperatures. The resulting curve was used to calibrate the calorimeter. Losses to the plate were found to be 0.00053 Btu/sec. °F. for the upstream calorimeter and 0.00023 Btu/sec. °F. for the downstream calorimeter. These values are about twice those reported by Cavers.

A series of three flux measurements was taken for each run, extending over an approximate period of two hours. During this time the plate-block differential* was not allowed to vary more than 0.02° F. Moreover, no electrical energy input adjustments were permitted during the run; thus the calorimeters had to reach a steady state before data were recorded. This requirement is believed to account largely for the precision obtained. The average plate-block differential during the

---
* The average of the difference between the calorimeter block temperature and the plate temperature at four intervals spaced 90° about the block (Figure 7, N).

run was used to correct for the losses to the plate, which were generally less than 2 per cent of the net flux.

The vertical gradient along the inner wall of the calorimeters was carefully kept less than 0.3° F. per foot during the calibrations and measurements. Unavoidable exceptions to this were encountered during three runs at high flux with the upstream calorimeter wherein a high gradient indicated excessive heat flow into the calorimeter from the upper oil bath. In these cases an appropriate correction was applied by measuring the change in plate-block differential with jacket gradient while maintaining a constant electrical energy input to the calorimeter. In the worst case the resultant correction was only 0.5 per cent of the net flux.

Prior to each flux measurement a run was made with air and plates at the temperature of the upper plate for the subsequent flux run. Appreciable losses after corrections were found to exist during these isothermal runs and are attributed mainly to energy being transferred in more than one direction. The bulk of this loss is probably out to the sides of the channel. Accordingly, the flux during the isothermal run is subtracted from the gross flux to obtain the net experimental value. These corrections were 3.6 per cent of the thermal flux in the worst case. Of all the corrections applied, the "isothermal" correction is the most difficult to interpret. It is believed that the losses out the sides are greater during the flux measurements than during the isothermal runs, in which case the correction is only a step in the right direction.

Experimental Results:

The tests made and the conditions imposed are listed in Table I, along with the gross and net fluxes and corrections. No temperature or velocity traverses were taken, the emphasis having been placed on the calorimetric work.

From the values for the net fluxes the Nusselt number was calculated for both calorimeters during each run:

$$Nu = \frac{4 \dot{Q} y_0}{\Delta t \, k} \tag{21}$$

The value of y_0 here is the actual plate separation (± 0.3 per cent) at the calorimeters as determined from the channel geometry and precise measurements of the plate profiles. Δt is the difference between the upper and lower plate temperatures measured with a pair of thermocouples imbedded in the copper plates directly upstream of each calorimeter.

The Reynolds number was obtained from the expression:

$$Re = \frac{2 y_0 \rho U}{\eta} = \frac{2 y_0 \rho f_7 (u_m)}{\eta} \tag{22}$$

where y_0 is the plate separation just ahead of the calorimeter, and U is the bulk velocity. Since no velocity traverses were made, U was obtained from a known experimental correlation between U and u_m, the peak velocity measured by a pitot tube. The correlation has been prepared from past integrations across the channel, and can be applied with ± 0.5 per cent accuracy. Figure 6 shows the curve used, along with the test points. It is, of course, not a universal

relationship, but is applicable specifically to the equipment used. The density, ρ, was calculated from the actual channel pressure.

Nu is shown as a function of Re on a log-log scale in Figure 7. The curves recommended by Prandtl (14) and McAdams (9) were derived for flow of heat in both normal and axial directions. Their values of Nu are accordingly high, but the slopes are similar. A maximum deviation of 2.5 per cent is indicated. At the lowest Re the value of u_m is known only to ± 2 per cent, the accuracy of the pitot tube determination at 15 feet per second.

It is noteworthy that the Nusselt numbers for the down-stream calorimeter are consistently higher than those for the up-stream calorimeter. At the latter the block and plate were flush, but at the former the block was recessed from 0.2 to 0.7 per cent of the total plate separation. A transient increase in turbulence may therefore explain the higher transfer rate for the downstream calor-imeter.

The equation of the curve for $Re > 10{,}000$ is:

$$Nu = 0.0328 \, Re^{0.728} \tag{23}$$

Since the fluid used here is air, Equation (23) is the final form of the experimental relationship. If it were assumed that the Nusselt number varied with the 0.4 power of the Prandtl number (7), then Equation (23) might be rewritten:

$$Nu = 0.0377 \, Re^{0.728} Pr^{0.4} \qquad (24)$$

However, Equation (24) remains to be proved by experiments with fluids having different Prandtl numbers.

As is explained by Cavers, the calorimetric measurements until now have fallen into three groups, each of which represents an improvement in design and technique over the previous group. These are:

Group I   - With original calorimeter design - tests with 60° F. plate differential

Group II   - With reduced plate separation to cut down air leakage - tests with 10° F. and 30° F. differential

Group III - With reduced block thickness - single test with 30° F. differential

The tests described herein should be classified under the new heading:

Group III-A - Same as Group III, but with improvement of steady state operation - tests with 30° F. and 60° F. differential

The calorimetric results for the first three groups are shown in Figure 8. For purposes of comparison Group III-A is shown as the solid curve obtained from Figure 7. It is clear that the major improvement in the calorimetric measurements resulted from reducing the plate separation. Losses from non-uniform flow (air leakage) appear to

have been excessive in the Group I measurements. Despite the re-
duced plate separation such losses may still be occurring to a
lesser extent. Past experience may thus provide a clue as to the nature
of the losses incurred during the isothermal runs described above.

From the point distributions for all groups it appears that
the curvature at the lowest Reynolds numbers is pronounced. A
Reynolds number of 10,000 roughly marks the beginning of the transi-
tion region between turbulent and laminar flow for this particular
equipment, and the curve begins to lose accuracy below that value.

Figure 9 shows the Fanning friction factor f as a func-
tion of Reynolds number for the heat transfer equipment. The fric-
tion factor for this figure was calculated indirectly from several
values of u_m, the peak velocity, using the expression:

$$f = \frac{y_0 \left(-\frac{dP}{dx}\right)}{\rho v^2} \tag{25}$$

$\frac{dP}{dx}$, as well as v, was obtained from a graphical correlation
with u_m. The $\frac{dP}{dx}$ correlation is shown in Figure 10, which was
drawn up for a standard y_0 value of 0.700 inches. A standard value
had to be chosen because of the unavoidable bowing of the copper
plates. For a given mass rate of flow $\frac{dP}{dx}$ varies inversely with the
third power of y_0, whereas u_m varies inversely with the first
power. To use the chart, therefore, u_m must be converted from the
average to the standard plate spacing, and the corresponding value
of $\frac{dP}{dx}$ from the chart then corrected back to the average plate
spacing. ρ is the average air density for the tests used to obtain

the $\mathcal{U}$ and $\frac{dP}{dx}$ correlations.

The Reynolds number was calculated for the same values of from Equation (22), which is repeated here for convenience:

$$R_e = \frac{2 y_0 \rho f_7 (u_m)}{\eta} \qquad (26)$$

The curve of Figure 9 is not quite a straight line, but it does increase in curvature at the lower Reynolds numbers, as does Figure 7. The copper plates were oil-and-dust-free, and were polished to a smoothness, $\mathcal{l}$, of 25 microinches (13), or a relative roughness, $\frac{l}{y_0}$, equal to 0.000035.

Application of Results:

On the basis of the Nusselt correlation established by the Group III-A thermal flux measurements, Cavers' symmetrical and smoothed values of total conductivity for Tests 40, 41, 45, 46 (Group II) and 60 (Group III) have been corrected. Test 44 has also been corrected and included. The validity of the eddy quantities obtained during the latter test are questioned by Page (8) but the results are indicated here because they are the only Group II measurements available at a nominal velocity of 90 feet per second. The friction-distance parameter $y+$ has been corrected for revised pressure gradients arising from the variation in plate separation (15). The relationship expressed by Equation (19) is explored by plotting the function $\frac{\epsilon_c}{K}\left(\dfrac{1}{1-\frac{2y_d}{y_0}}\right)$ versus $y+$ in Figure 11. The equation of the straight portion of the curve is:

$$\frac{\epsilon_c}{K}\left(\frac{1}{1-\frac{2y_d}{y_0}}\right) = 0.353(y+) - 2.9 \qquad (27)$$

the slope of which is slightly less than that found by Cavers:

$$\frac{\epsilon_c}{K}\left(\frac{1}{1-\frac{2y_d}{y_o}}\right) = 0.372(y+) - 2.9 \tag{28}$$

The smoothed symmetrical total viscosities have also been corrected on the basis of the improved $\frac{dP}{dx}$ values. $\frac{\epsilon_m}{V}\left(\frac{1}{1-\frac{2y_d}{y_o}}\right)$ is plotted against $y+$ in Figure 12. The equation of the straight portion of the curve in the turbulent core is:

$$\frac{\epsilon_m}{V}\left(\frac{1}{1-\frac{2y_d}{y_o}}\right) = 0.396(y+) - 2.9 \tag{29}$$

which differs slightly from the von Kármán expression:

$$\frac{\epsilon_m}{V}\left(\frac{1}{1-\frac{2y_d}{y_o}}\right) = 0.40(y+) \tag{30}$$

It is worthy of note that the ordinate intercepts for Equations (27) and (29) are equal.

The plot of $\frac{\epsilon_m}{V}\left(\frac{1}{1-\frac{2y_d}{y_o}}\right)$ versus $y+$ by Cavers included isothermal runs as well. Figure 12, however, was limited to the runs with thermal flux so that the degree of scattering could be compared with that in Figure 11. Nikuradse's data for flow of water in pipes are also shown for comparison (16). Figures 11 and 12 are repeated in Figures 13 and 14, the $y+$ scale being magnified to show the nature of the scattering at low values. In the region of the laminar layer, $0 < y+ < 5$, the curves have been drawn through the theoretical value of unity. In the buffer layer, $5 < y+ < 30$, the curve for $\frac{\epsilon_m}{V}\left(\frac{1}{1-\frac{2y_d}{y_o}}\right)$ has been drawn to

correspond with that determined in Tests 110 and 111. (See Part II of this thesis.) The continuous velocity determinations made during these tests are believed to provide unusually accurate values of ϵ_m.

Neither Figure 11 nor Figure 12 shows complete correlation, but the pattern of deviation at higher values of $y+$ is noticeably similar for the two cases. As a matter of engineering interest it is convenient to define a prediction factor as the fraction of the distance from wall to midstream, $y+_m$, over which Equations (27) and (29) may be applied. Choice of the point of incipient deviation, $y+_c$, is arbitrary. If the allowable deviation of the ϵ function is arbitrarily set at 2 units, a plot of the prediction factor $\frac{y+_{c1}}{y+_m}$ $\left(= \alpha \right)$ versus the Reynolds number results in the curve of Figure 15. If the allowable deviation is 20 per cent the prediction factor $\frac{y+_{c2}}{y+_m}$ $\left(= \beta \right)$ is higher, as in Figure 16. The usefulness of these charts therefore depends on the accuracy of prediction required. They should not be used indiscriminately, but they do show that the correlation falls off with increasing Reynolds number.

Figure 16 shows the function obtained by combining the relationships of Figures 13 and 14 by means of Equation (20). The curves shown for Tests 46 and 60 were corrected for revised pressure gradient and thermal flux values, and represent experimental results based on the relationship:

$$\frac{\epsilon_c}{\epsilon_m} \cdot \frac{\nu}{K} = \frac{\overset{\circ}{Q}}{\tau C_p g} \frac{1}{\frac{\partial t}{\partial u}} \tag{31}$$

The values of $\frac{\partial t}{\partial u}$ used in Equation (31) were obtained by Cavers in his original work, and have not been corrected for impact temperature

rise. However, this effect is small ($\Delta t = 0.014^{\circ}$ F.) at 15 feet
per second and 30° F. plate differential (17), the nominal conditions
at which both tests were carried out.

Comparison of these curves with those obtained by Cavers
shows an improvement in agreement of the experimental work with the
predicted values. This improvement supports the validity of the
intermediate steps leading to the relationship of Equation (20). The
predicted curve has less curvature and one less point of inflection
than that initially proposed by Cavers. The universality of Equation
(20) in the turbulent zone also appears to be limited to that which
would be predicted from Figure 15 at $Re = 9800$. The greatest error
shows up in the region $0 < y+ < 30$, the region of the laminar
and buffer layers. The wide deviation there is believed to result
from the limited accuracy of velocity measurements during Tests 45
and 46.

Conclusion:

By a series of painstaking measurements a Nusselt-Reynolds
macroscopic correlation of high precision has been found for the case
of heat transfer across a turbulently flowing air stream. This
should supplement earlier correlations by Prandtl and others, which
applied to situations of non-uniform flow. Below Reynolds numbers
of 10,000 the reliability of the correlation falls off.

If velocities, temperatures, and plate separation are
measured with the apparatus, it should now be possible to determine
accurately the eddy properties at any point in the stream without
the need of additional measurements. In the buffer layer the Reynolds

analogy is the least certain. A study in this region will be of considerable value in establishing the certainty of the correlations above.

Part II
==

Introduction:
--

In Part I of this thesis values were found for the total
viscosity and total conductivity during earlier experimental work
on the heat transfer equipment. These values depended upon accurate
measurements of shear, thermal flux, velocity gradient, and temper-
ature gradient. Corrections were made to past values of shear and
thermal flux, using graphical correlations established by a series
of runs. The former temperature gradients were also corrected for
impact temperature rise, which becomes significant at the higher
velocities (17). No attempt was made, however, to improve the
values originally used for the velocity gradients, which were based
upon hours of painstaking laboratory work.

Part II of this thesis deals with two methods which may
be of use in the accurate determination of mean velocity gradients.
The von Kármán velocity distribution law has proved useful in pre-
dicting velocities. When used to predict velocity gradients and
eddy values, however, it results in a discontinuity at the boundary
between the turbulent core and the buffer layer. In the actual case
one might expect the eddy values to vary continuously.

The earlier measurements of velocity were carried out by
measuring the energy dissipated from a wire in accordance with King's
Equation (18):

$$a + b u^{1/2} = \frac{I^2 R_{hw}}{R_{hw} - R_a} = \phi \tag{32}$$

where μ is the mean air speed past the wire, I is the current, R_{hw} is the wire resistance, R_2 is the wire resistance with no current flowing, and a and b are constants. The wire is mounted on support needles as shown in Figure 4 and may be brought within a few diameters of a parallel surface. The suitability of the hot-wire method for determining velocities has been thoroughly investigated (19,20,21,22). Corrsin (23) in particular has dealt with the theoretical behavior of the hot wire in the presence of temperature gradients.

According to Equation (32) a plot of ϕ versus $\mu^{1/2}$ should be a straight line. In actual practice this is not quite so, and the relationship must be explored by a pitot tube calibration at several different velocities. The experimentally determined relationship is then valid anywhere in the channel if the turbulence level is small or constant across the channel. The effect of varying turbulence level has been investigated by Laufer (22), who made an intensive study of velocity distribution in a 5 inch by 60 inch by 23 foot long channel.

Velocity measurements are likely to show a scattering of points near the wall where the gradient is steepest. This scattering is caused by the change in calibration of the hot-wire with time and by the uncertainty in determining channel position. Several factors, including the deposition of dust on the wire, may bring about a change in calibration. The rate of change is unsteady, and may be constant for many operating hours before changing suddenly. To minimize the effect of this unsteadiness a series of rapid measurements would be desirable. The error in channel position could be minimized by taking these measurements continuously.

Two approaches are generally made to hot-wire anemometry,
(1) the constant-resistance method, in which the wire temperature is
kept constant, and (2) the constant-current method in which the
current through the wire is held constant and the temperature
changes with the heat dissipation (19). Both methods are adaptable
to continuous velocity recording.

The Constant-Resistance Continuous Recording Anemometer:

The constant-resistance anemometer now used in the heat
transfer channel has been described by Page (8), and is a 0.0005-
inch diameter 5/16 inch long platinum wire mounted on a probe as
in Figure 4. In the circuit of Figure 18 it acts as one arm of a
Wheatstone bridge. Current through the bridge is supplied by an
external power source, such as a storage battery. A variable re-
sistor controls the current through the bridge circuit, and a Leeds
and Northrup galvanometer indicates when the bridge is balanced, i.e.,
when the wire is at the desired temperature. The hot-wire voltage
E_{hw} is directly measured by a potentiometer. The current is
determined by measuring the voltage E_s across a standard resistor
in series with the hot wire. The ratio $\dfrac{E_{hw}}{I}$ is equal to the hot-
wire resistance R_{hw}. R_a is obtained by measuring the wire resist-
ance at the air temperature with a Mueller bridge. As described by
Page, the determination of the Wheatstone bridge balance point is
a matter of statistical judgment, since the instantaneous velocity
is continually fluctuating.

The main feature of the continuous method (25) makes use
of the galvanometer to control current input to the bridge by re-
flecting light onto a photoelectric cell. The cell drives a power

amplifier whose output lies partly in series with the battery source.
As a control mechanism the system is stabilized by an inductive
coupling made from an ordinary output transformer. The primary is
inserted in series with a bias resistor in the amplifier circuit,
the secondary being in series with the galvanometer itself. Any
fluctuation in the galvanometer position is thereby strongly opposed
by the coupling without loss of sensitivity to the galvanometer.

For continuous recording, the probe is driven across the
channel at a desired speed (from 0.01 to 0.1 inches per minute) by
an electrical motor with adjustable reduction gears, Figure 19. The
potential across the standard resistor R_s is measured by means of
two potentiometers in series. A Leeds and Northrup K-2 potentiometer
provides most of the opposing voltage, while a Leeds and Northrup
White potentiometer provides the residual voltage. A recording gal-
vanometer indicates the difference between the voltage across the
standard resistor and the combined voltage across the potentiometers.
This galvanometer is mounted in a Miller camera, Figure 20, which
records the galvanometer deflection on a 7-inch spool of sensitized
paper. Three other galvanometers are also used, one for the refer-
ence or base line, and two others for synchronizing signals from the
traversing gear and temperature bench. The deflection of all four
galvanometers may be simultaneously observed on the ground glass
screen of the camera during the actual recordings. The camera is
located near the potentiometers for convenience. The initial wire
position with respect to the wall is determined by sighting diagonally
into the channel with a cathetometer and measuring the object-image

separation. The wire position during the run may be followed through a Lucite window with a small telescope located directly opposite the probe outside the channel. A synchronizing button is depressed manually by the traversing gear observer at the instant of reading. As the voltage across the standard resistor changes, the White potentiometer setting is changed by the observer at the temperature bench so as to keep the Miller galvanometer within range.

The recording galvanometer is calibrated before each traverse. Use of the compensated stepwise White potentiometer means a constant galvanometer sensitivity over the measured range, and the calibration is therefore applicable as long as the K-2 setting is not changed appreciably. The Wheatstone bridge is balanced manually, and the recording galvanometer is brought to its natural rest point with the K-2 potentiometer. The White potentiometer is then reset to cause a deflection, which provides the necessary calibration.

To take the continuous measurement the Wheatstone bridge is put on automatic control, i.e., the power amplifier and inductive coupling are inserted into the circuit. The camera and traversing gear are started. As the wire moves across the channel, its position is checked by telescope every two thousandths of an inch. The wire observer records the position and sends a simultaneous synchronizing signal to the camera. When the recording galvanometer light reaches the extremity of the sensitized paper, the temperature bench observer changes the White potentiometer setting and records the new value. At the end of the run, the paper is developed and cut into pieces corresponding to each change of setting. The pieces are mounted on

coordinate paper at intervals determined from the calibration, as in Figure 21. This figure shows the residual voltage as a function of channel position. With a change of scale it becomes a residual current plot.

The circuit used tends to become unstable when large currents are furnished by the amplifier. For that reason the rheostat is periodically adjusted to keep the control current low. The control range for the photocell is sufficiently small that the difference between zero and full load from the amplifier calls for the Wheatstone bridge to be off balance by 1 microvolt.

Figure 22 shows the difference in the hot-wire fluctuations with the controller furnishing large and small average input currents, I_f . The subscript f denotes the fact that the input current is filtered pulsating d. c. current[*]. The filtering was inadequate, and for this reason a 120-cycle signal is superimposed on the tracks of Figure 22. The true amplitude of the 120-cycle signal does not show up on the tracks because the galvanometer is overdamped at frequencies higher than 10 cycles per second. The wave pattern of the control current was examined with a cathode ray oscilloscope, however, and the amplitude of the ripple current was found to be of the same order of magnitude as the d. c. component. If the control current is not constant during the run, some error may be introduced

- - - - - - - - - -

[*] Expedience led to the use of an available thyratron control circuit instead of a direct-current power amplifier. An improvised filter circuit was used to reduce the jagged wave pattern characteristic of a thyratron pulsating discharge (25).

in the calibration of the hot wire by the use of King's equation[*].
Because of the instability mentioned in the preceding paragraph,
however, the control current is purposely kept small. The error
due to fluctuations is therefore negligible. The chief significance
of Figure 22 is the exaggerated fluctuation pattern obtained when
the controller is "working hard". It would therefore not be suitable
for a study of deviating velocities, even though the recording gal-
vanometer were capable of responding at higher frequencies.

To measure temperatures the same wire used for determin-
ing velocities becomes a resistance thermometer. The circuit is
of conventional four-lead design (24), and makes use of a Leeds and
Northrup Mueller bridge. By throwing a six-pole switch (Figure 18),
one can change readily from the velocity circuit to the temperature
circuit. Current through the wire from the Mueller bridge with the
maximum sensitivity button depressed is 3.0 milliamperes, enough to
raise its temperature appreciably. Indicated temperatures should
therefore be corrected for this effect as well as for the tempera-
ture rise due to the impact of the air on the wire (17). The velocity
measurements may be carried out with the wire at high enough a temper-
ature so that the corrections to R_a will be small as compared with
the value of $(R_{hw} - R_a)$ used in Equation (32). The measured

---

[*] For a sinusoidal wave pattern the average current, I_a, and the
amplitude of the superimposed alternating current, I_b, determine
the true power dissipation, which is:

$$\frac{1}{\Delta\theta}\int I^2 R_{hw}\, d\theta = \frac{R_{hw}}{\theta}\int(I_a + I_b \sin\omega\theta)^2\, d\theta = \left(I_a^2 + \frac{I_b^2}{2}\right) R_{hw}$$

where θ is the unit of time. The average current is:

$$\frac{1}{\Delta\theta}\int I\, d\theta = \frac{1}{\Delta\theta}\int(I_a + I_b \sin\omega\theta)\, d\theta = I_a$$

Hence the apparent dissipation is:

$$I_a^2 R_{hw}$$

velocities are therefore not affected by neglecting these correc-
tions. With a high gradient across the stream R_a may vary by several
per cent of $\left(R_{hw} - R_a\right)$. In such a case a temperature traverse
must be taken with the velocity traverse. Two measurements are
needed to obtain R_a with a Mueller bridge, one with leads normal,
the other with leads reversed (24). Consequently two separate temper-
ature traverses are required if continuous values of R_a are to be
obtained.

The Mueller bridge operates at a much lower current than
the Wheatstone bridge, so that the energy dissipated from the wire
is far less. A galvanometer of higher sensitivity is thus required
to detect off-balance, the recording galvanometer being inadequate
for the purpose. During the temperature traverse the bench observer
therefore follows the deflection of the highly sensitive Mueller
bridge galvanometer[*], records the instant of its rest point with
his synchronizing button, and writes down the value of the bridge
setting. His synchronous signals are later compared with the signals
recorded by the wire observer to obtain the resistance as a function
of position in the channel. Figure 23 is such a record. With a
wire which has been calibrated at several temperatures smooth values
of the air temperature may be obtained.

The Constant-Current Continuous Recording Anemometer:

When the current is held at a fixed high value, the temper-
ature of the hot wire varies with position in stream. The circuit
for this type of anemometer is shown in Figure 24. The total resistance

---

[*] Sensitivity of this galvanometer when critically damped is 5 mm. per
microvolt at a distance of one meter.

of the circuit must be large compared with the change in R_{hw} so that the current will not fluctuate. The hot-wire voltage is recorded continuously, just as the voltage across the standard resistor was recorded for the constant-resistance anemometer. The recorded track may be read at the natural rest point of the recording galvanometer. Consequently the calibration of the galvanometer may be dispensed with, and the K-2 potentiometer may be used alone. When the galvanometer reaches the extremity of the sensitized paper, the potentiometer setting is changed by the observer at the temperature bench. Since this change is not stepwise, as was the case with the White potentiometer, a portion of the track is invalid. The synchronizing button is therefore depressed during the adjustment so as to void the reading during that interval. The fluctuating track is averaged by a smooth line. The natural rest point track of the galvanometer is known, although imaginary, and it intersects the smoothed curve at a point on the record which may be identified with channel position. A constant current run is shown in Figure 25, cut into three strips laid side by side for convenience in illustrating.

The temperature traverses may be taken in the manner previously described, or the run may be repeated twice with successively lower currents. In the latter case the hot-wire resistance may be extrapolated to zero current, where R_{hw} equals R_a. The latter method was used here for exploratory reasons, but possesses no special advantages unless a study of the hot-wire fluctuations is desired. As the current is successively decreased, the device becomes less of an anemometer, and more of a resistance thermometer. The application of King's equation in such a case becomes highly involved (23).

Experimental Results:

Partial velocity traverses were made at 30 feet per second, both with and without a 30° F. differential across the plates. Table II lists the operating conditions for all tests. Owing to the presence of a 0.5 inch sphere five feet upstream in the channel (26) no attempt was made to obtain complete traverses. The wire was calibrated against a pitot tube at four different velocities during each run. It was found that the complete calibration took several times as long as the combined set of three traverses. The latter required about half an hour.

In Tests 110 and 111 the calibration was made twice, once before and once after the actual traverses. No significant change in calibration was found for these tests. The values of Φ and $u^{1/2}$ measured during the calibrations are listed in Table III.

Tests 109 and 110 were constant-current runs at three different currents. The current setting used to calibrate the wire was inadvertently 10 per cent below the highest value used during the three traverses. The error thus introduced may be effectively corrected in two ways, either (a) by comparing Φ as a function of I for a constant channel position during the run, or (b) by calibrating at different currents and applying the slope $\frac{\partial \Phi}{\partial I}$ to obtain Φ at the desired current. Both methods give results within the accuracy of the calibration. The correction applied can be expressed by the following empirical modification of King's equation:

$$\frac{I^2 R_{hw}}{(R_{hw} - R_a)^{1.04}} = a + b u^{1/2} \tag{33}$$

Wave patterns for two constant current runs at 10 milli-
amps are shown in Figure 26, and indicate the residual fluctuating
voltage across the hot wire. 26 (a) and 26 (c) are taken from
Test 109, where a flux existed across the channel. 26 (b) and 26 (d)
are from Test 110, and isothermal run. In the isothermal runs the
deviating voltage is small. In the runs with flux, however, the
deviating voltage is appreciable, and must be attributed almost
entirely to temperature fluctuations. In other words the current
is so low that the wire has ceased to be an anemometer and behaves
as a thermometer.

The temperature fluctuation level ϑ may be defined (23)
as the r.m.s. deviating temperature divided by the difference be-
tween the average point temperature and the average temperature at
the center of the stream. ϑ plays an important part in the statis-
tical study of the heat transfer mechanism. It is analogous to the
turbulence level, defined as the r.m.s. deviating velocity divided
by the mean directional velocity. A rough integration of Figure 26
(a) and 26 (c) indicates temperature fluctuation levels for Test 109
of 0.3 per cent at $\frac{y}{y_o}$ = 0.991 and 1.0 per cent at $\frac{y}{y_o}$ = 0.916.

The velocity values are shown in Figure 27. Tests 123 and
124 were preliminary runs at the same nominal channel conditions as
the remaining tests but without knowledge of the wall position. The
latter has therefore been estimated from the velocity profile shape
alone. For Tests 109, 110, and 111, in which the wall position was
accurately known, appropriate values of $u+$ and $y+$ were calculated
and plotted in Figure 28. Of these Test 111, a constant-resistance
run, falls closest to the von Kármán curve. More significant, perhaps,

is the fact that the constant current runs indicate slightly lower
generalized velocities $u+$ than does the constant resistance run.
Interpretation of the data is dependent upon accurate shear as well
as velocity values. A few more tests would therefore be advisable
before coming to any conclusion about the relative merits of the
results obtained by the two methods.

By combining Equations (1), (3), and (5) the following
expression is obtained:

$$\frac{\epsilon_m}{\nu} \left(\frac{1}{1 - \frac{2y_d}{y_0}} \right) = \frac{\tau_0}{\eta} \left(\frac{1}{\frac{\partial u}{\partial y}} \right) \tag{34}$$

The right hand side of Equation (34) is plotted in Figure 29 as a
function of $y+$ for Tests 110 and 111. The discontinuity of the
von Kármán expression is seen to be neatly bridged at the half-way
point.

Discussion:

The fact that King's equation is not a universal function
has been realized by other investigators (19,21,22,25). Because the
wire is sensitive to total speed, rather than velocity, it may
respond somewhat differently near the wall where the turbulence level
is higher (22). Betchov and Welling (21) point out that ϕ increases
with temperature because of the variation in convective losses with
temperature along the wire axis (the "non-linearity" effect). They
have also examined the theoretical effect of conduction to the ex-
tremities of the wire but find that it is secondary.

In addition to the foregoing side losses there will be vary-
ing losses by radiation when the constant-current method is used.

Figure 30 shows the calculated effect of wire temperature on radiation losses from a 0.0005-inch diameter, 5/16-inch long wire to infinite parallel plates at 115° and 85° F., the emissivity factor being unity (27). In Figure 31 the variation in hot-wire energy dissipation with y_d is shown for constant-current Test 110 and constant-resistance Test 111. The variation in wire temperature with y_d during a constant-current run is indicated in Figure 32. In the absence of an experimental calibration the temperature coefficient for the wire was assumed equal to the known value for a platinum resistance thermometer.

By making use of the equation for potential flow from a line source to an infinite plane (28), the losses to the plate by molecular conduction have been calculated for constant-resistance Test 111, in which the wire temperature was approximately 255° F. Figure 33 shows these losses as a function of y_d .

Because the side losses are numerous, their analysis is a complex problem. The calibration and the run should therefore always be made at one constant resistance or one constant temperature. In this way the losses not covered by the elementary form of King's equation will cancel out. Equation (33) is an approximation, applicable only to the specific experimental case undertaken. It should not be used for precision work.

In Figure 21 an abrupt change in slope of the track is noted close to the wall. This characteristic was observed in both the constant-resistance and the constant-current runs, and appears to be the result of added loss from the wire by conduction to the

wall. For the constant-resistance runs this change occured at y_d = 0.0075 inch, or 15 wire diameters. For the constant-current runs the change occured at y_d = 0.0085 inch, or 17 wire diameters. These values may be roughly compared with the theoretical conduction losses for still air shown in Figure 33. Despite the rise of temperature near the wall in Figure 32 the effect of conduction during the constant-current runs becomes significant only 2 wire diameters further away from the wall than is the case with the constant-resistance method.

Laufer (22) noted an apparent decrease in velocity close to the wall of a 5-inch channel at R_e = 12,300. He ascribed this effect to a large rise in the turbulence level at a $\frac{y}{y_o}$ value of 0.995. In the 0.7-inch channel the phenomenon was not observed, and would be obscured by the conduction effect at y_d < 17 diameters.

Conclusion:

The hot-wire methods described herein yield smooth velocity profiles which are reproducible within $\pm$ 1 per cent in the buffer layer, regardless of which method is used. The wall position is believed known within two wire diameters, and the velocities may be readily extrapolated to zero at the wall. The thermal flux appears to have no effect on the velocity profile within the range of accuracy.

The total viscosity values obtained in exploratory Tests 110 and 111 evenly bridge the gap left by the von Kármán buffer-layer theory, but are about 10 per cent higher than those of earlier tests carried out in a conventional stepwise manner. When they are

used with total conductivities to predict the Reynolds analogy, as
in Part I, Figure 17, of this thesis, a plot with less curvature and
one less point of inflection is obtained. A series of continuous
temperature and velocity measurements in the buffer layer with the
sphere removed from the channel upstream may show that the one re-
maining inflection is unwarranted.

It appears that the constant-resistance and constant-
current methods are equally applicable in studies of mean velocity
distribution, although the second method is somewhat more direct.
Neither method as described herein is applicable to the study of
deviating velocities, but the constant-current method may be of
value in measuring deviating temperatures.

Continuous traverses should be especially useful in the
study of non-uniform flow past heated shapes, such work having been
the subject of recent experimental investigation in this laboratory
(29).

NOMENCLATURE

a intercept of King's equation

b slope of King's equation

C_p specific heat at constant pressure, Btu/lb.°F.

E_{hw} electrical potential across hot wire, volts

E_s electrical potential across standard resistor, volts

f Fanning friction factor

$f_n(\ )$ a function of, the subscript n being used to distinguish one function from another

$f_n'(\ )$ the derivative of a function with respect to its argument

g gravitational acceleration, ft./sec.^{2}

I current through hot wire, amperes

I_{dc} current through wire from battery, amperes

I_f r.m.s. current through wire from controller (partially filtered) amperes

I_a time average of current in hot wire, amperes

I_b amplitude of ripple current in hot wire, amperes

k thermal conductivity, Btu.ft./sec.ft.^{2}°F.

l length of hot wire, ft.

Nu Nusselt number, defined by Equation (21)

Nu' local (point) Nusselt number, defined herein as $\lim \dfrac{\dot{Q}}{\Delta t}\dfrac{\Delta y}{\epsilon_c}$

P pressure, lb./ft.^{2}

Pr molecular Prandtl number, equal to $\dfrac{\nu}{K}$ (For this paper a constant = 0.709 to within 0.2%)

Pr' local (point) turbulent Prandtl number, defined herein as $\dfrac{\epsilon_m}{\epsilon_c}$

$\dot{Q}$ rate of heat transfer per unit area, Btu./ft.^{2}sec.

Re Reynolds number

Re' local (point) Reynolds number, defined herein as

R_{hw} resistance of hot wire, ohms

r_w radius of hot wire

R_a resistance of hot wire with no current flowing, ohms

R_x variable resistance in anemometer circuit, ohms

R_{24} code number on C.I.T. Chem. Eng. dwg. 25824

T_6 ditto

T_{13} ditto

T_{14} ditto

t mean (time average) temperature at a point, °F.

t_{hw} temperature of hot wire, °F.

t_p temperature of a plate, °F.

u mean (time average) velocity at a point, ft./sec.

u^* friction velocity, ft./sec., defined as $\sqrt{\dfrac{\tau_0}{\rho}}$

u^+ dimensionless velocity parameter, defined as $\dfrac{u}{u^*}$

U bulk velocity, ft./sec., defined as $\displaystyle\int_0^1 u \, d\left(\frac{y}{y_0}\right)$

u_m maximum mean velocity, ft./sec.

u_{mc} maximum mean velocity, corrected to standard y_0 of 0.0583 ft. ($\approx$ 0.700 in.)

x distance in the direction of flow, ft.

y distance above lower plate, ft.

y_d distance below upper plate, ft.

y_0 height of channel, ft.

y^+ dimensionless distance parameter, defined as $\dfrac{y_d \, u^*}{\nu}$

y^+_c point of incipient deviation from Equations (27) and (29)

$y^+_{c_1}$ point where deviation exceeds 2 units on $\dfrac{\epsilon_m}{\nu}\left(\dfrac{1}{1-\frac{2y_d}{y_0}}\right)$ or $\dfrac{\epsilon_c}{\chi}\left(\dfrac{1}{1-\frac{2y_d}{y_0}}\right)$ scale

$y^+_{c_2}$ point where deviation exceeds 20 per cent on $\dfrac{\epsilon_m}{\nu}\left(\dfrac{1}{1-\frac{2y_d}{y_0}}\right)$ or $\dfrac{\epsilon_c}{\chi}\left(\dfrac{1}{1-\frac{2y_d}{y_0}}\right)$ scale

α prediction factor

β prediction factor

$\underline{\epsilon}$ exchange quantity, ft.^{2}/sec.

ϵ_m eddy viscosity, ft.^{2}/sec.

$\underline{\epsilon}_m$ total viscosity, ft.^{2}/sec.

ϵ_c eddy conductivity, ft.^{2}/sec.

$\underline{\epsilon}_c$ total conductivity, ft.^{2}/sec.

η absolute viscosity, lb.sec./ft.^{2}

K thermometric conductivity, ft.^{2}/sec.

ν kinematic viscosity, ft.^{2}/sec.

ρ density, lb.sec.^{2}/ft.^{4}

ϑ temperature fluctuation level defined as the r.m.s. deviating temperature divided by

τ shear, lb./ft.^{2}

τ_o shear at a wall, lb./ft.^{2}

$\theta\!\!\!\!-$ the expression $\dfrac{\underline{\epsilon}_m}{\nu}\left(\dfrac{1}{1-\frac{2y_d}{y_o}}\right)$

θ time, seconds

ω angular velocity, defined here as 2π x frequency

χ dimensionless stability parameter, defined as $y_d^2\,\dfrac{\partial u}{\partial y}\,\dfrac{1}{\nu}$

ϕ the dependent variable in King's equation, defined as

$$\frac{I^2 R_{hw}}{R_{hw}-R_a}$$

REFERENCES

1. Reynolds, O., Proc. Lit. Soc. of Manchester, Vol. 14; 1875 (Oct. 6, 1874) (also Papers on Mechanical and Physical Subjects, Vol. 1, Paper No. 14, p. 81, University Press, Cambridge, England; 1900)

2. Prandtl, L., Physik. Zeitschr., 11, 1072 (1910)

3. Taylor, G. I., Brit. Advis. Comm. Aeronaut., Rep. and Mem. 272 (May 1916)

4. von Kármán, Th., Trans. A. S. M. E., 61, 705 (1939)

5. Boussinesq, J., Essai sur la theorie des eaux courantes, Memoires presentes par divers savanta a l'Academie des Sciences de l'Institut de France, Vol. 23 (1877)

6. Cavers, S. D., Ph. D. Thesis, California Institute of Technology (1951)

7. Jakob, Max, Heat Transfer, Vol. I, John Wiley & Sons (1949)

8. Page, Franklin, Ph. D. Thesis, California Institute of Technology (1950)

9. McAdams, W. H., Heat Transmission, McGraw-Hill (1942)

10. Bakhmeteff, B. A., The Mechanics of Turbulent Flow, Princeton University Press, (1941)

11. Rouse, Hunter, Elementary Mechanics of Fluids, John Wiley & Sons (1946)

12. Billman, G. W., Ph. D. Thesis, California Institute of Technology (1948)

13. Corcoran, W. H., Ph. D. Thesis, California Institute of Technology (1948)

14. Prandtl, L., Physik. Zeitschr., 29, 487 (1928)

15. Wilford, D. B., Student Report No. 401, Department of Chemical Engineering, California Institute of Technology (1951)

16. Nikuradse, J., VDI -Forschungsheft No. 356 (1932)

17. Berry, V. J., Student Report No. 300, Department of Chemical Engineering, California Institute of Technology (1949)

18. King, L. V., Phil. Trans. Roy. Soc., London, A214, 373 (1914)

19. Willis, J. B., Review of Hot Wire Anemometry, Australian Council for Aeronautics Report (Oct. 19, 1945)

20. Betchov, R., Proc. Kon. Ned. Akad. v. Wetensch. Amsterdam, 52, 195 (1949)

21. Betchov, R. and Welling, W., Proc. Kon. Ned. Akad. v. Wetensch. Amsterdam, 66, 432 (1950)

22. Laufer, John, Nat. Advisory Comm. Aeronaut. Tech. Note 2123 (July 1950)

23. Corrsin, Stanley, Nat. Advisory Comm. Aeronaut. Tech. Note 1864 (April 1949)

24. American Institute of Physics, Temperature, Its Measurement and Control, Reinhold (1941)

25. Sherwin, R. M., Student Report No. 405, Department of Chemical Engineering, California Institute of Technology (1951)

26. Wilford, D. B., Student Report No. 404, Department of Chemical Engineering, California Institute of Technology (1951)

27. Walker, W. H., Lewis, W. K., McAdams, W. H., and Gilliland, E. R., Principles of Chemical Engineering, McGraw-Hill (1937)

28. Muskat, M., Flow of Fluids Through Porous Media, McGraw-Hill (1937)

29. Billman, G. W., Mason, D. M., and Sage, B. H., Chem. Eng. Prog., 46, 625 (1950)

LIST OF FIGURES

Figure 1. Essential Features of the Apparatus

Legend: A. Upper Copper Plate
           B. Lower Copper Plate
           C. Blower
           D. Air Heater
           E. Air Entrance

Figure 2. Sectional Drawing of Channel

Legend: A   B   Oil Baths
        C,D,E   Oil Bath Seal and Channel Closure
        H,K   Supports for Upper Bath and Plate
        J,G   Ways for Traversing Gear
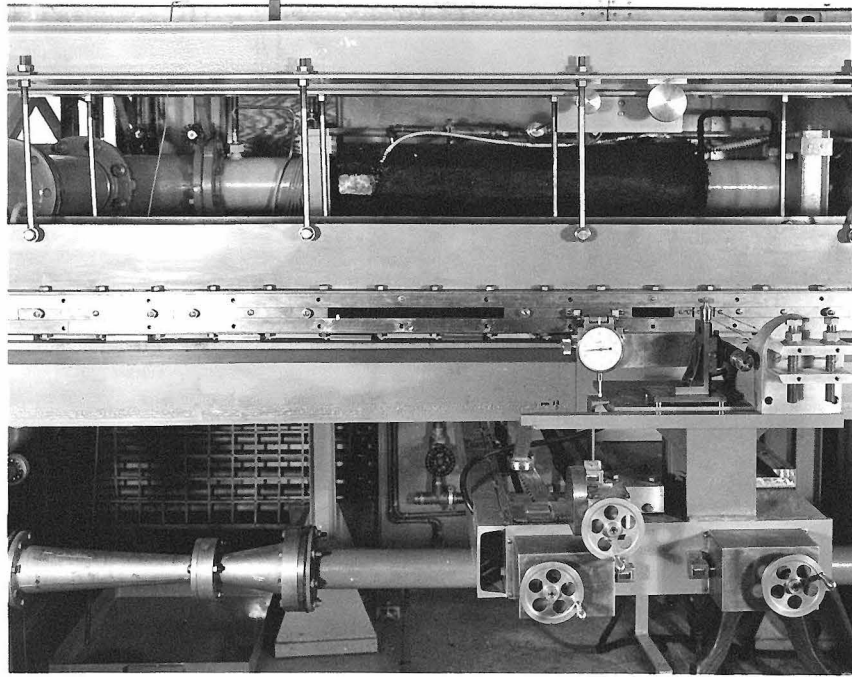
Figure 3. View of Traversing Gear and Channel, with
Side Blocks Partly Removed
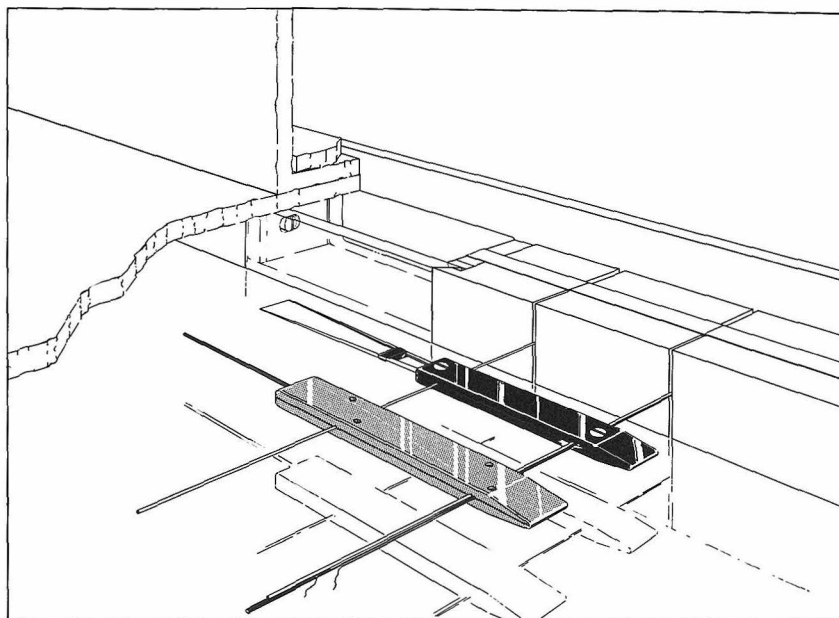
Figure 4. The Thermanemometer
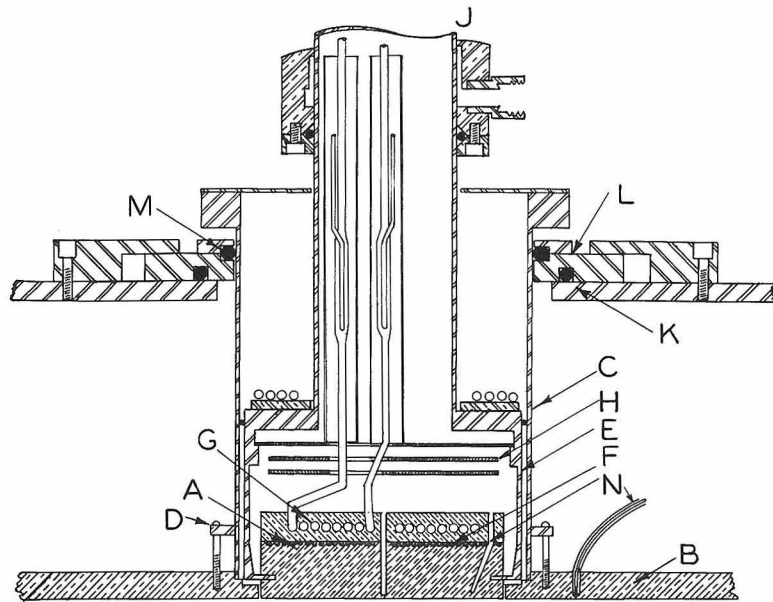
Figure 5. The Calorimeter

Legend: A. Copper Block
B. Copper Plate (Upper)
C. Outer Jacket
D. Fastening Screws
E. Inner Jacket
F. Manganin Heater
G. Cooling Coils (not required)
H. Radiation Shields
J. Upper Jacket
K,L,M. Oil Seal
N. Plate-Block Thermowells
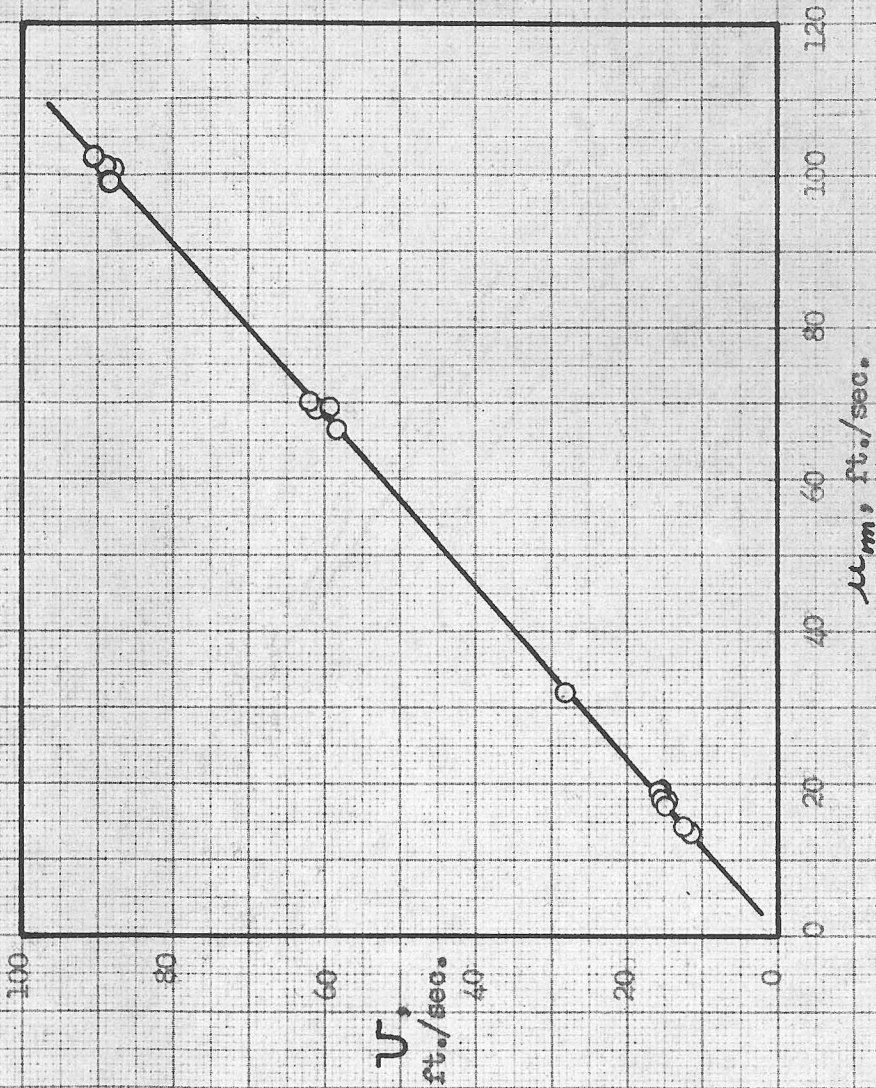
Figure 6. Experimental Correlation of the Bulk Velocity with the Peak Velocity
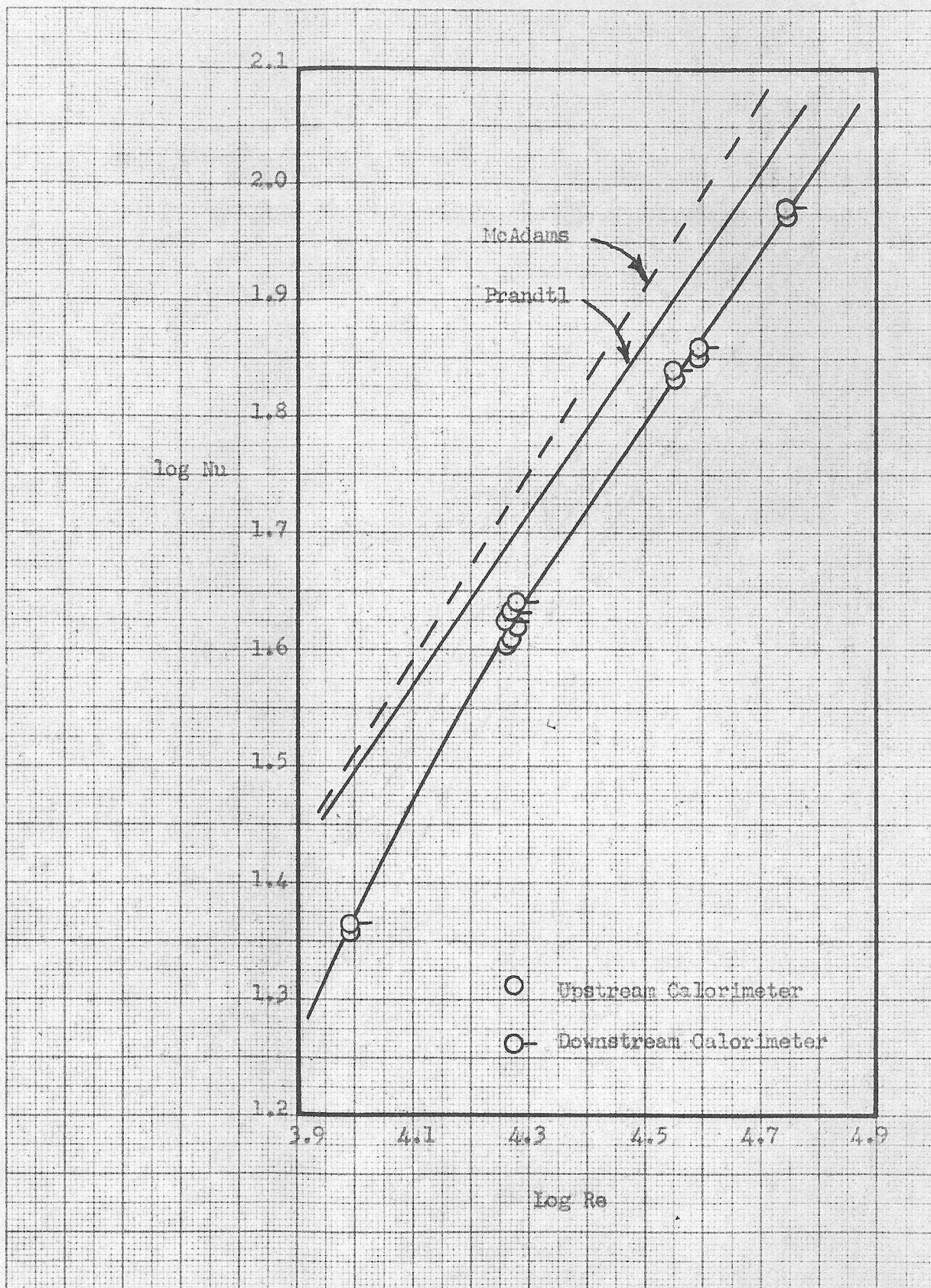
Figure 7. Log Nusselt Number as a Function of
Log Reynolds Number
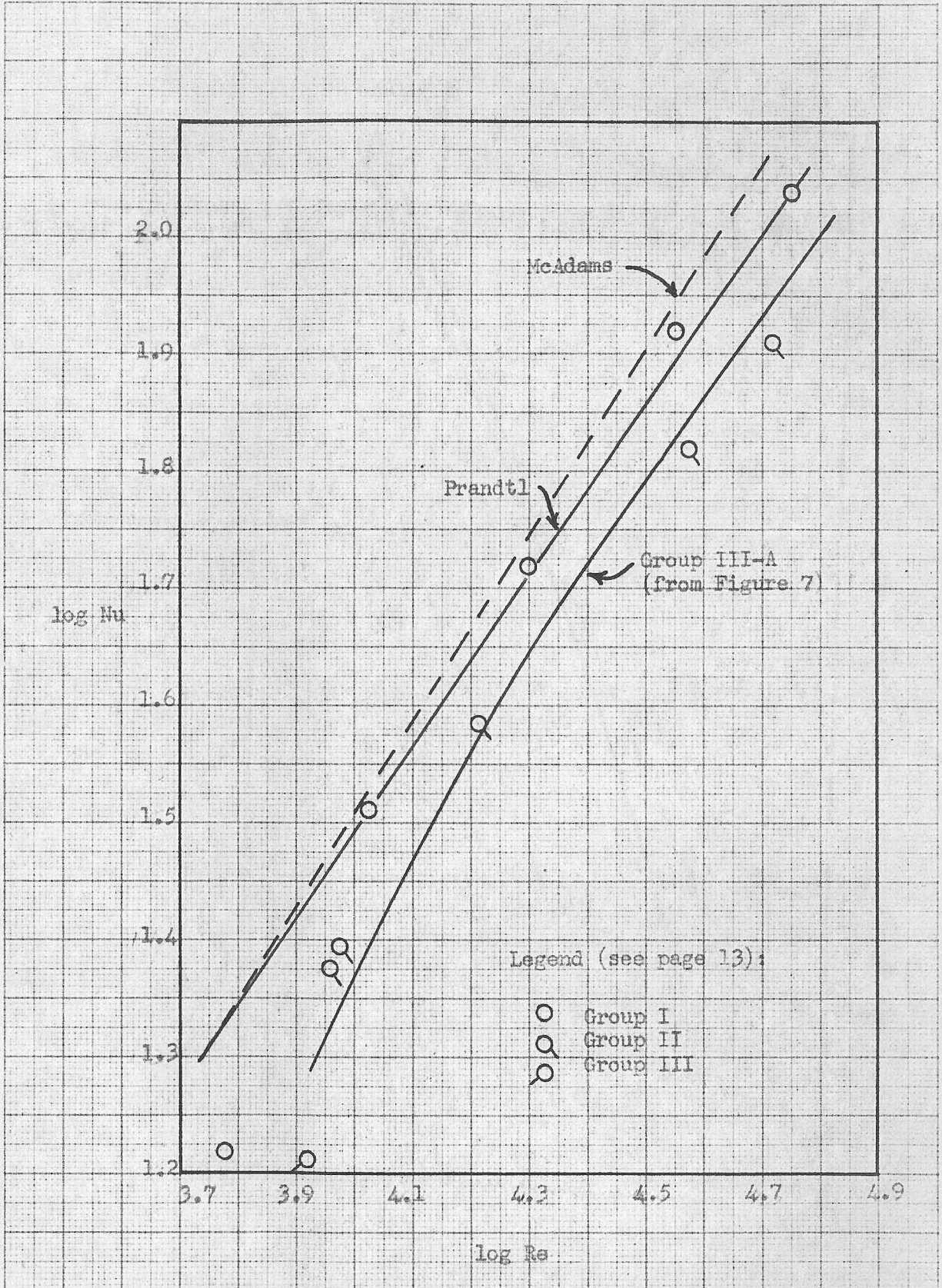
Figure 8. Comparison of Results with Earlier Calorimetric Data
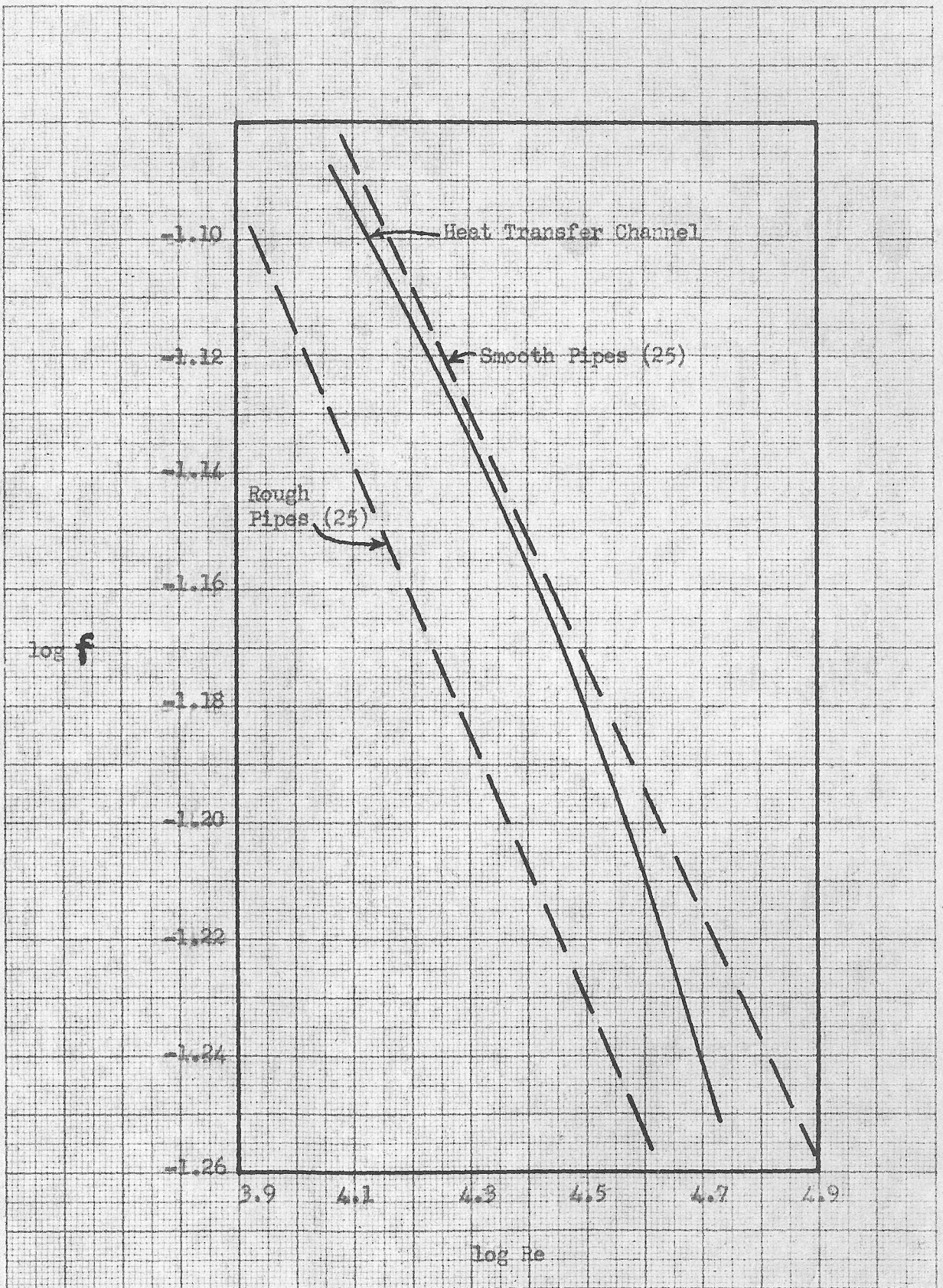
Figure 9. Log Friction Factor as a Function of log Reynolds Number
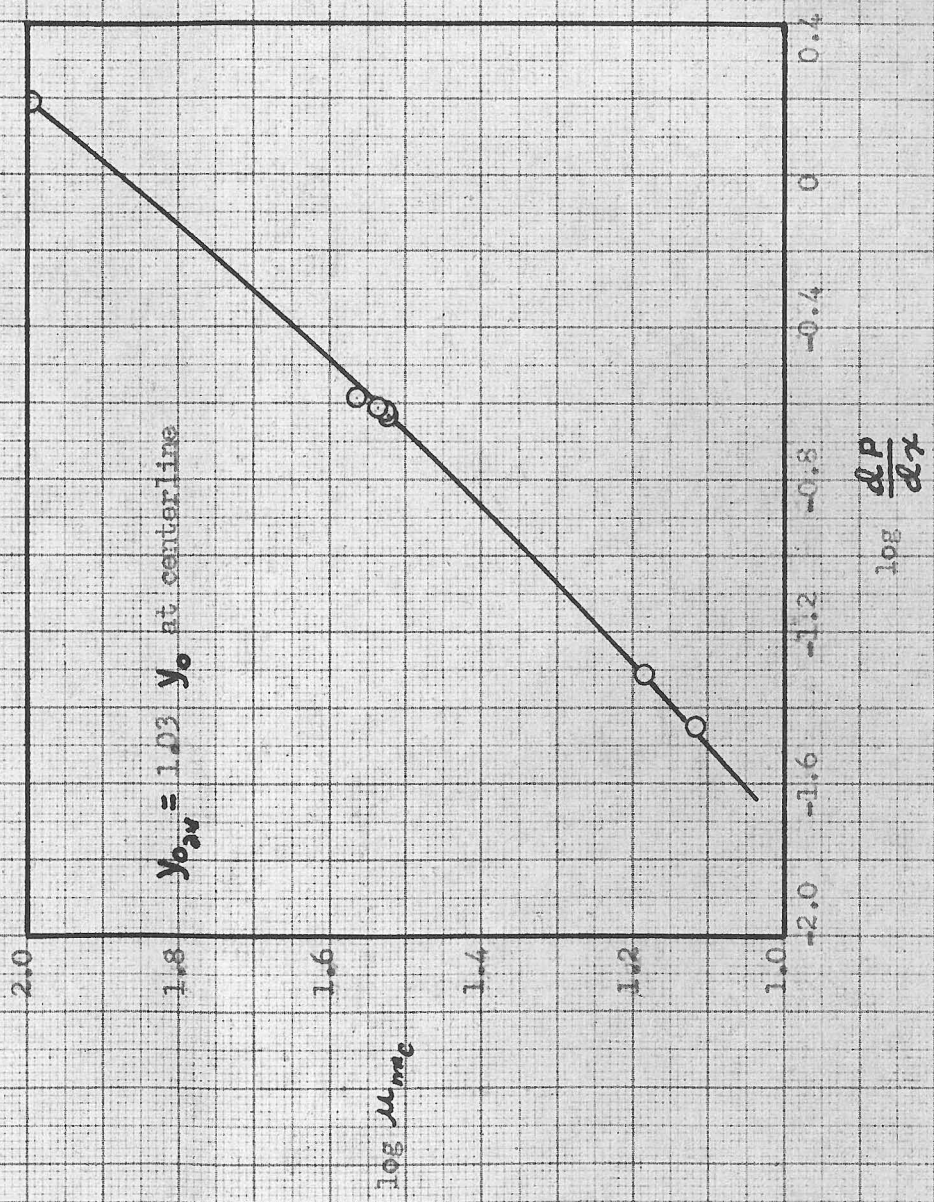
Figure 10. Correlation of Channel Pressure Gradient with Peak Velocity for $y_o = 0.700$ Inches
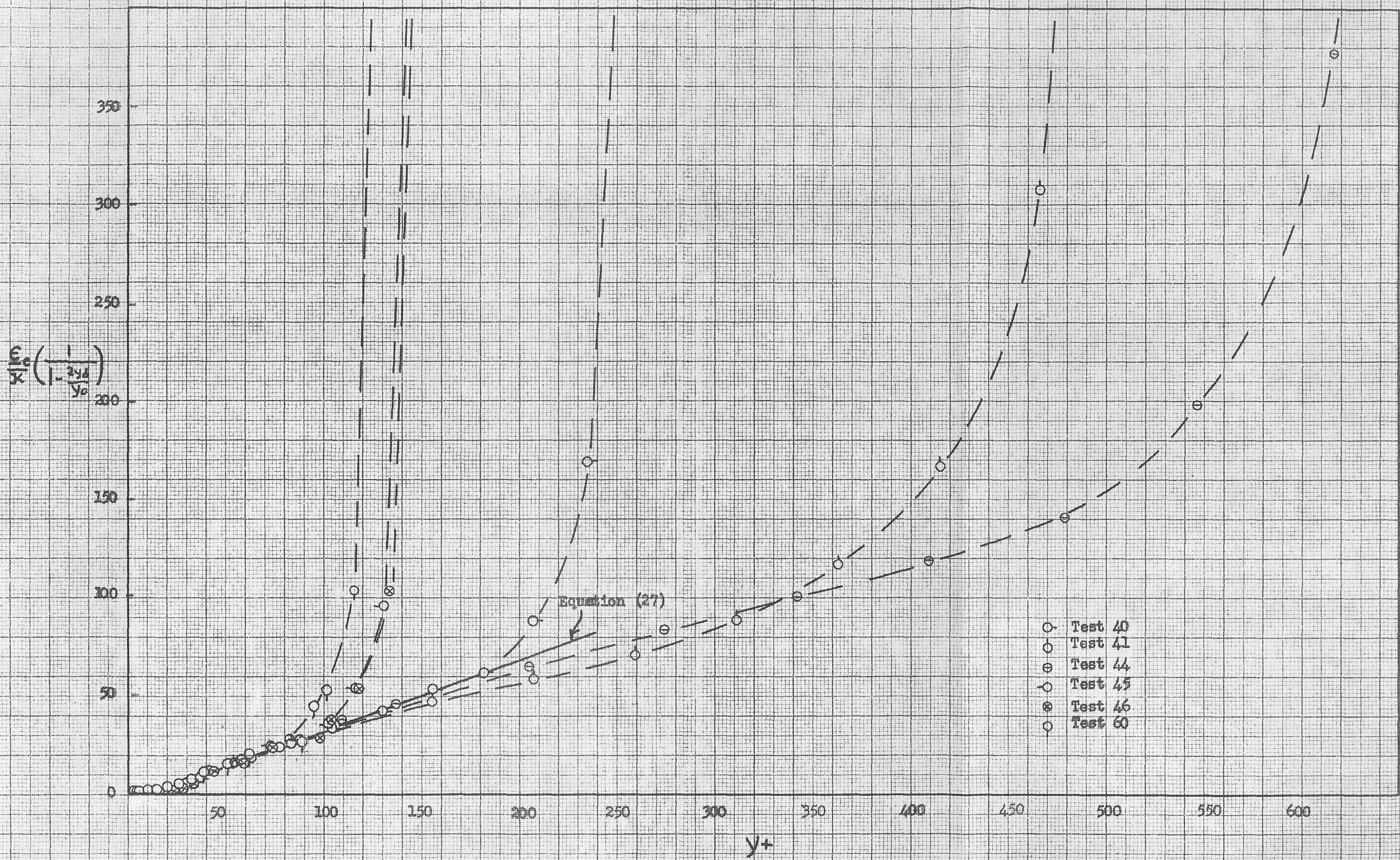
Figure 11. $\dfrac{\epsilon_c}{\kappa}\left(\dfrac{1}{1-\dfrac{2y_d}{y_0}}\right)$ as a Function of $y+$
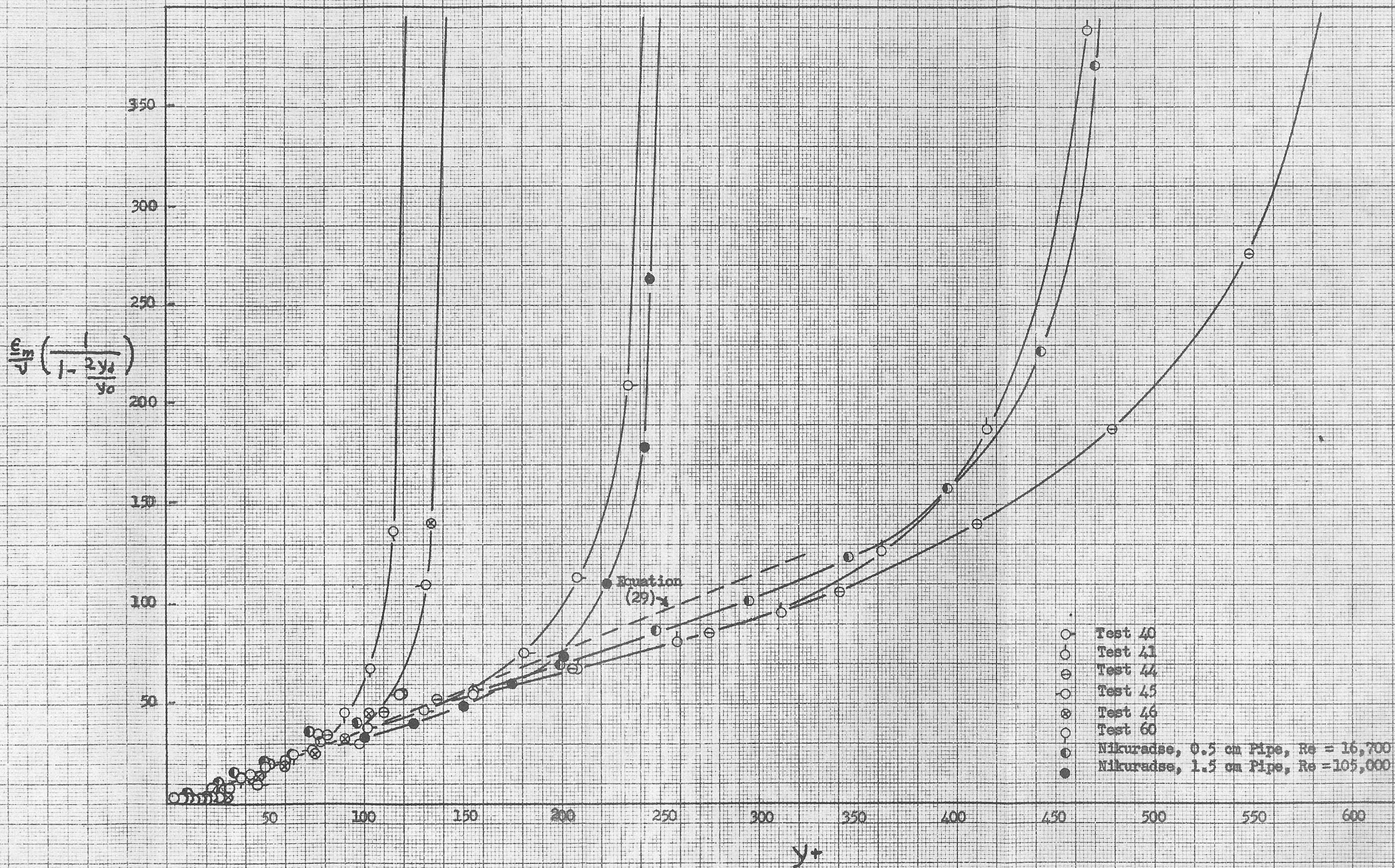
Figure 11.

Figure 12. $\frac{\varepsilon_m}{\nu}\left(\frac{1}{1-\frac{2y_d}{y_o}}\right)$ as a Function of $y+$

Figure 12

Figure 13. $\frac{\epsilon_c}{K}\left(\frac{1}{1-\frac{2y_d}{y_o}}\right)$ as a Function of $y+$ (Enlarged Scale)

Figure 13
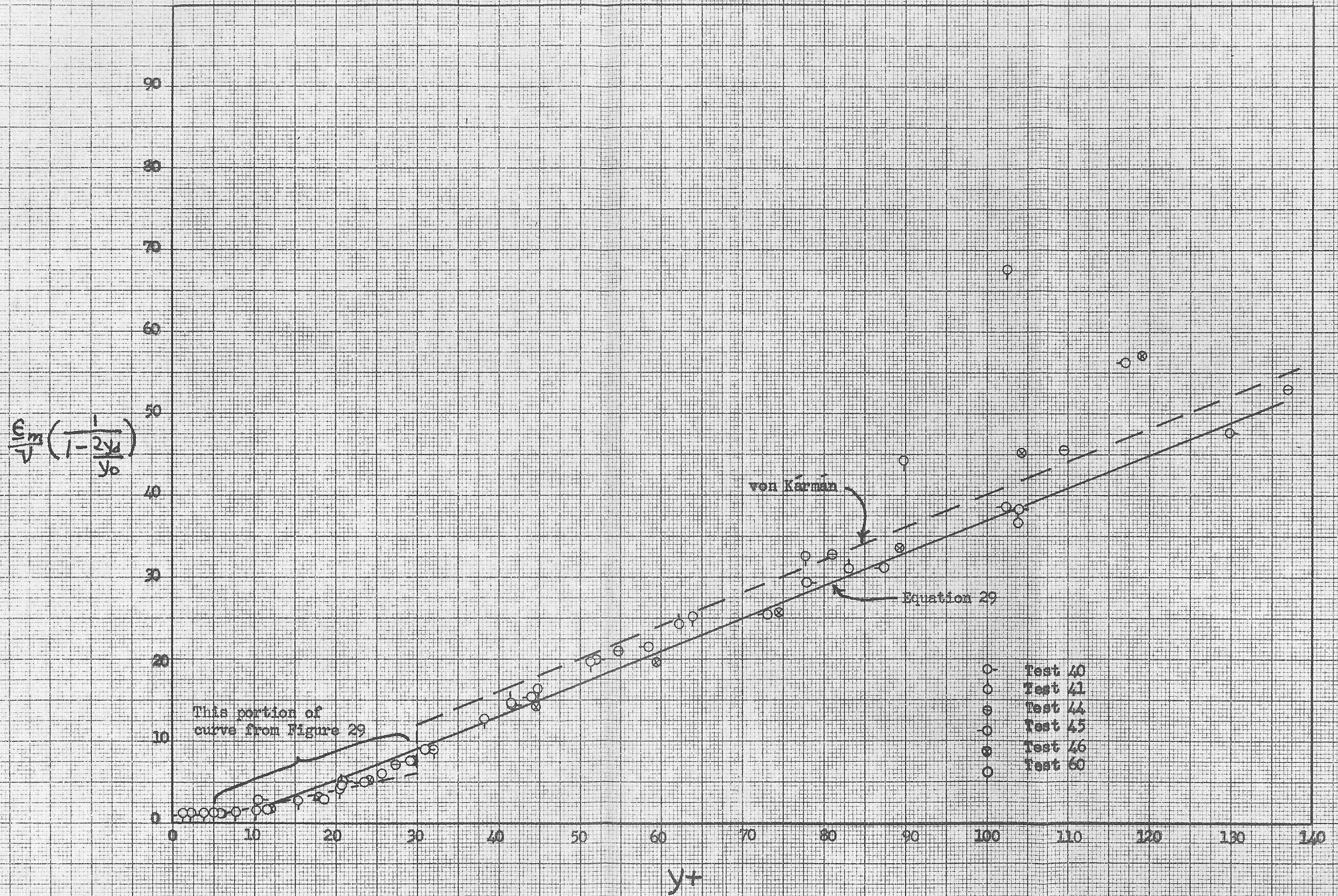
Figure 14. $\frac{\epsilon_m}{\nu}\left(\frac{1}{1-\frac{2y_d}{y_o}}\right)$ as a Function of $y+$ (Enlarged Scale)
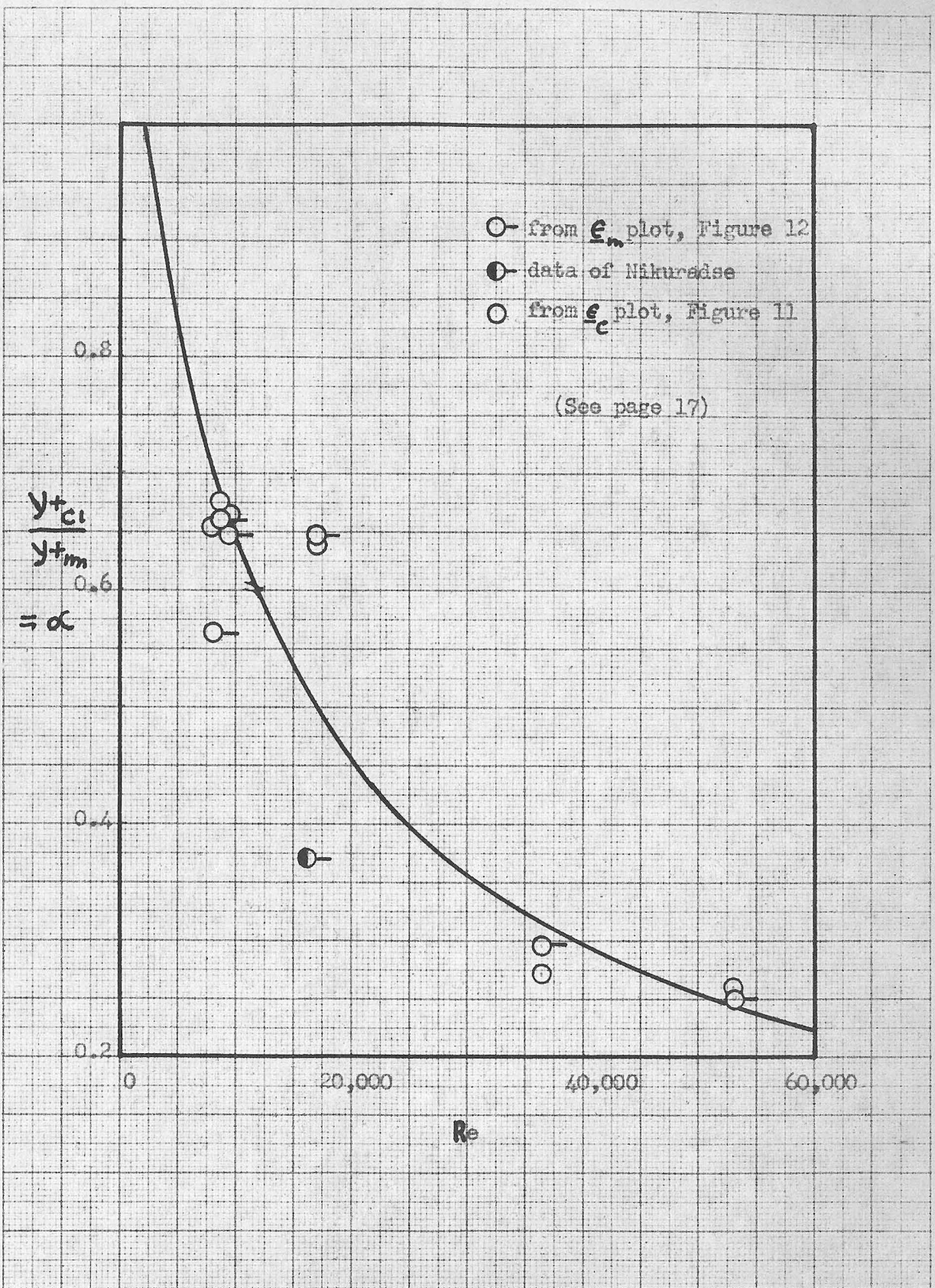
Figure 14

Figure 15.   Prediction Factor α as a Function of Reynolds Number
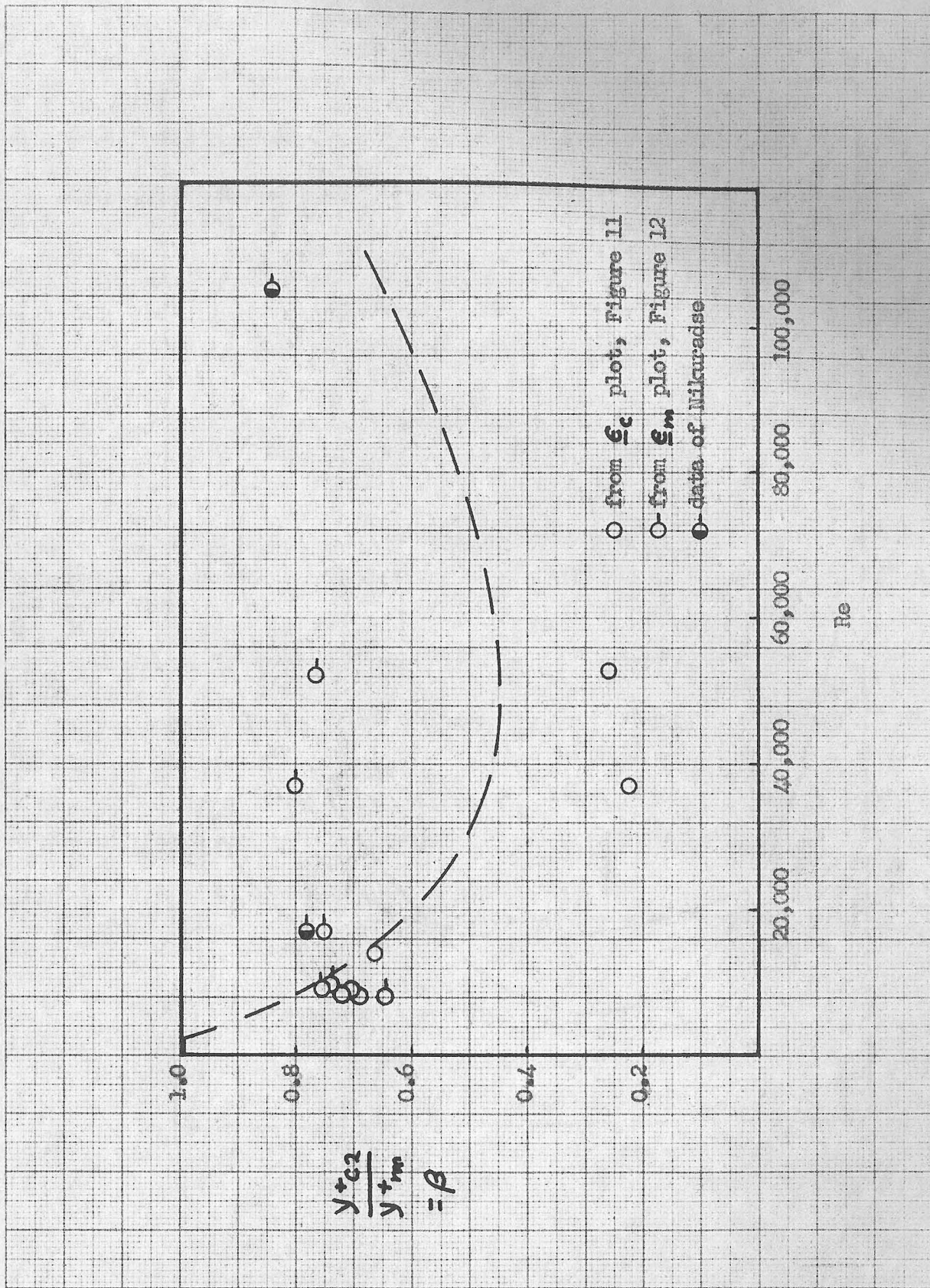
Figure 16. Prediction Factor as a Function of Reynolds Number
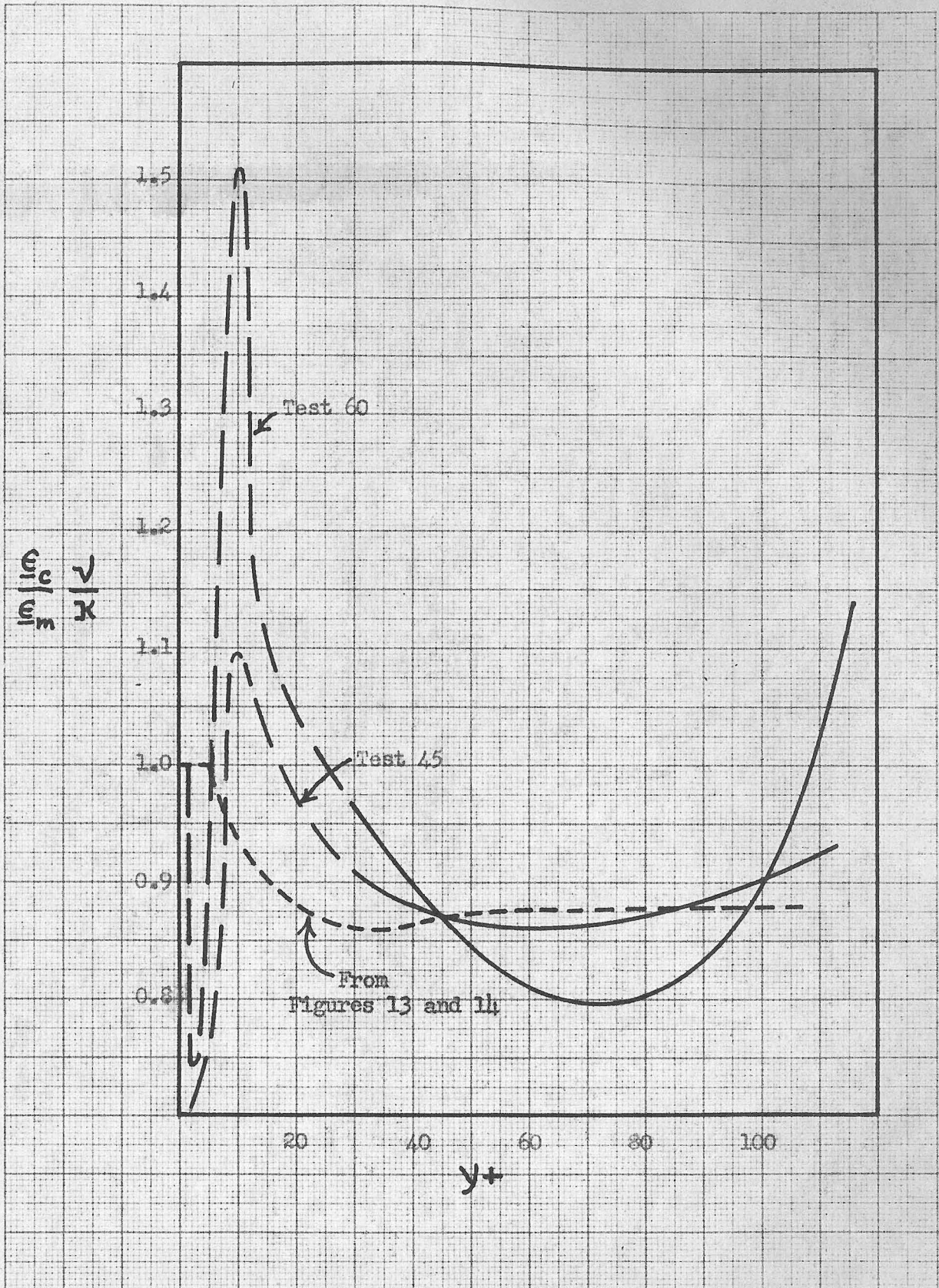
Figure 17. The Reynolds Analogy
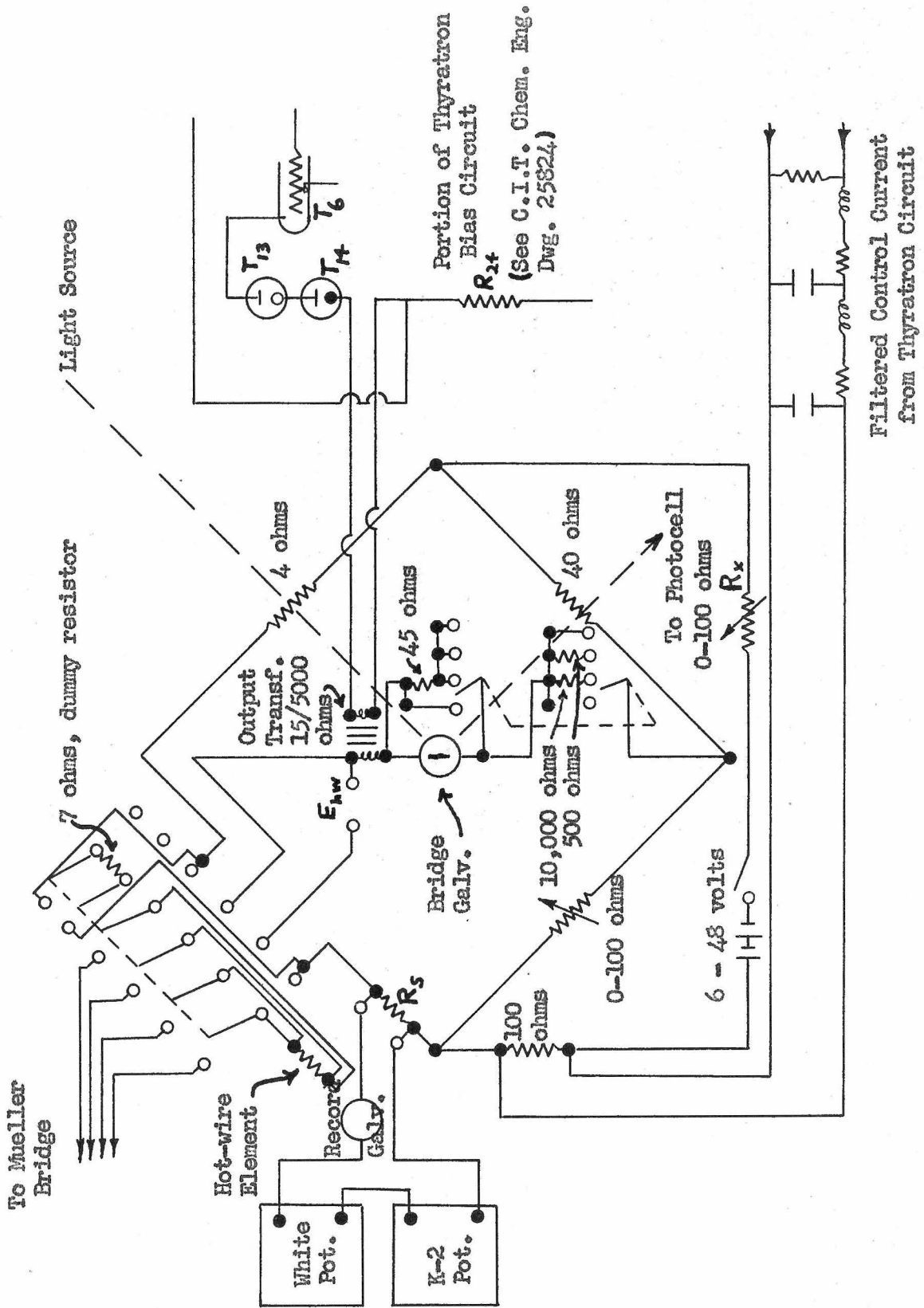
Figure 18. Circuit for Constant-Resistance Continuous Recording Anemometer
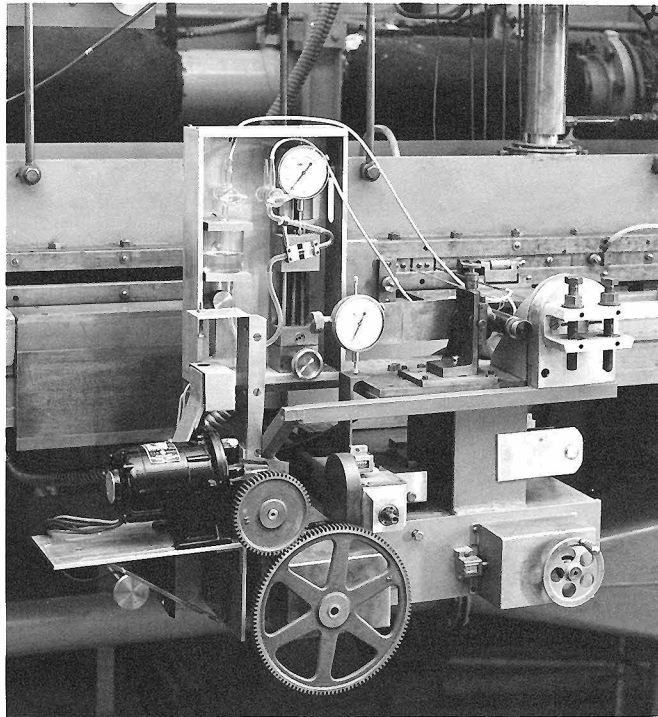
Figure 19.   Traversing Gear with Motor Drive
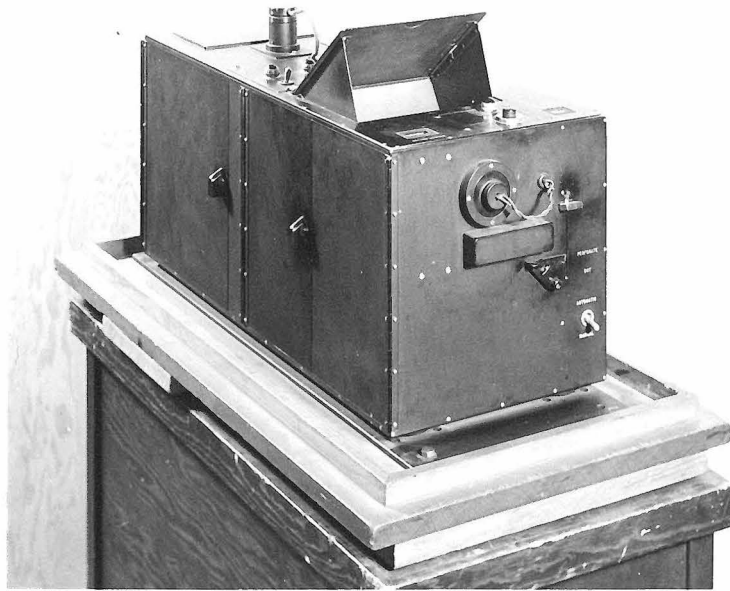
Figure 20. The Miller Camera
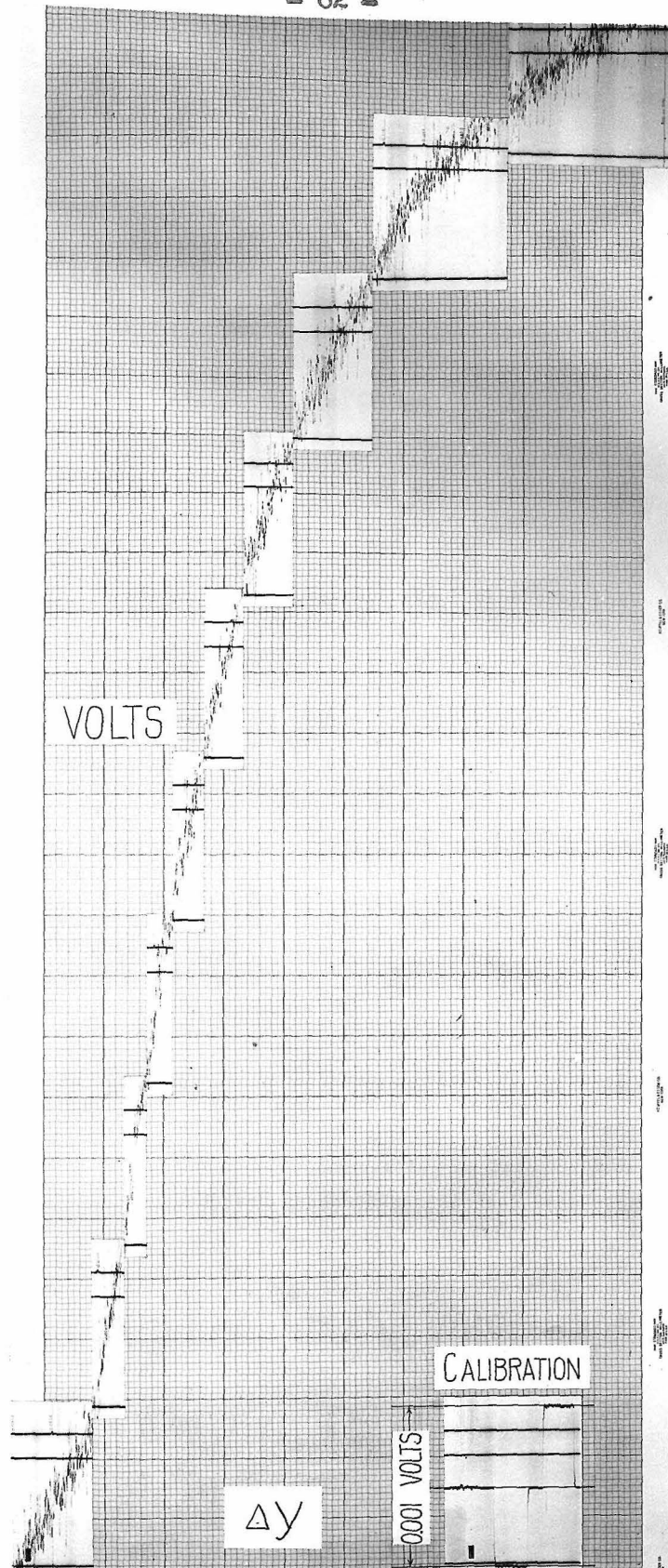
Figure 21. Constant-Resistance Track, $y/y_0 = 0.992$ to
$y/y_0 = 0.930$
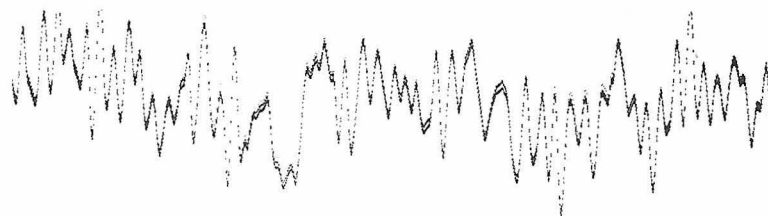
(a) $y/y_o = 0.92$ $I_{dc} = 90$ ma. $I_f = 20$ ma.

(b) $y/y_o = 0.92$ $I_{dc} = 105$ ma. $I_f = 5$ ma.
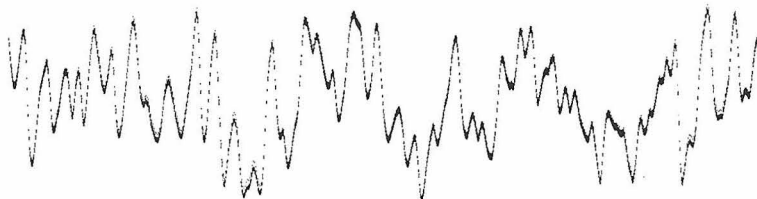
(c) $y/y_o = 0.93$ $I_{dc} = 80$ ma. $I_f = 15$ ma.
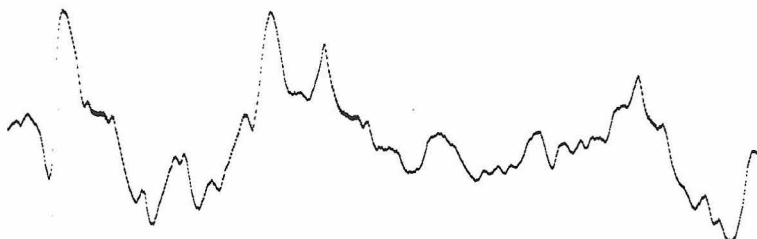
(d) $y/y_o = 0.98$ $I_{dc} = 92$ ma. $I_f = 3$ ma.

Figure 22.   Residual Hot-Wire Current Tracks at Fixed
Positions in Channel.   Paper Speed = 6 ft./min.
($\frac{1}{2}$ scale)

Base Line	(Idle Track)	R_R	Δy, Dial Reading
		5.6847	0.0950
			0.0956
		5.6845	0.0981
		5.6842	0.1008
			0.1025
		5.6840	
			0.1048
		5.6838	0.1073
			0.1090
			0.1118
		5.6836	
			0.1140
			0.1170
			0.1192
		5.6834	0.1220
			0.1250
			0.1280
		5.6832	
			0.1300
			0.1325
		5.6831	0.1352
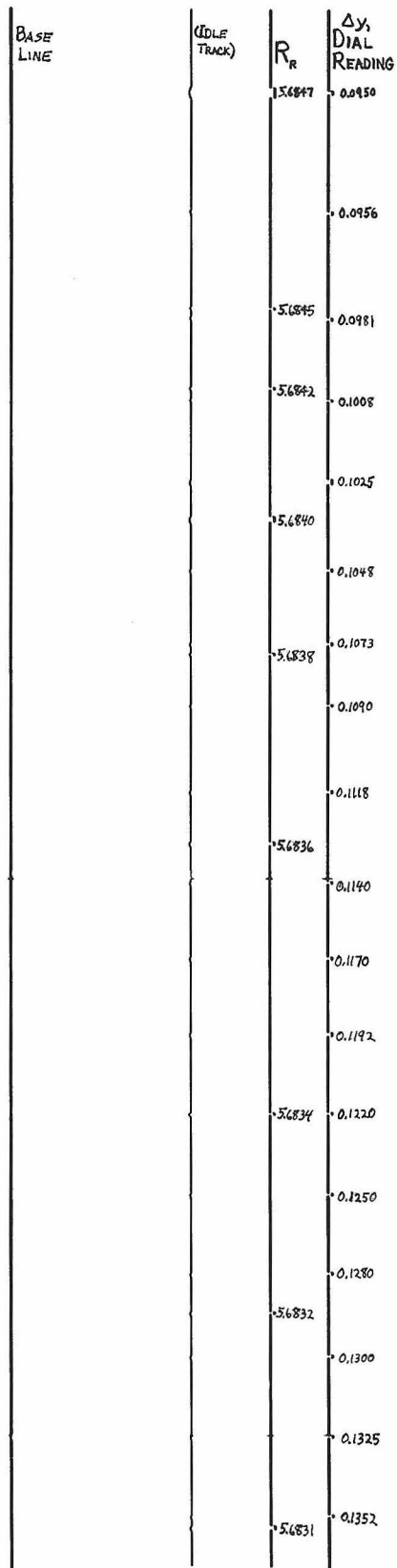
Figure 23. Typical Temperature Track. Paper Speed @ 3
in./min.   (approx. $\frac{1}{2}$ scale)
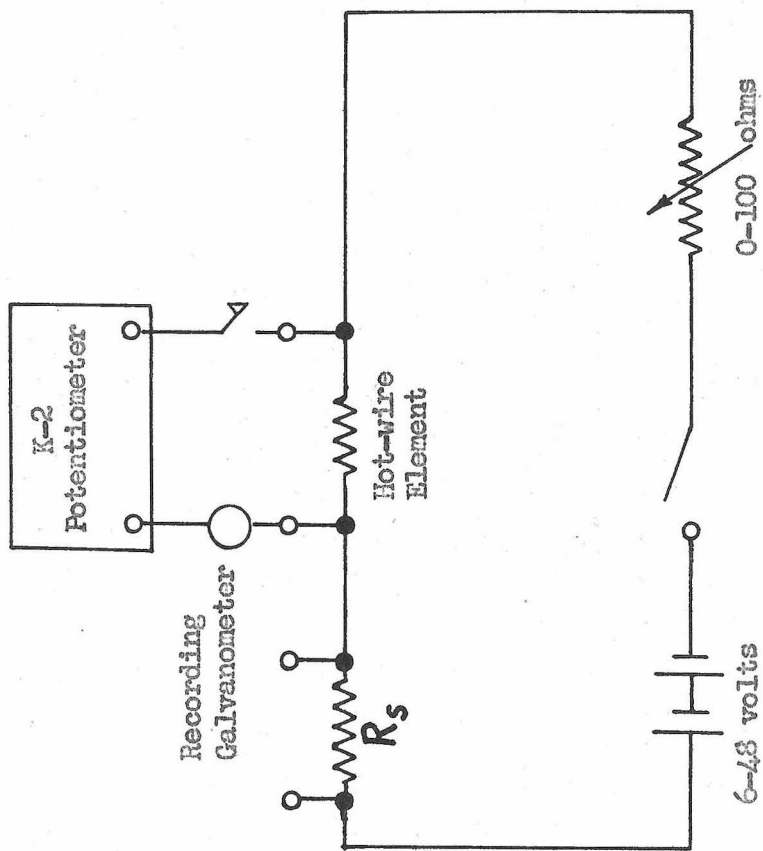
Figure 24. Circuit for Constant-Current Continuous
Recording Anemometer

BASE LINE

$\longrightarrow E_{RW} \longrightarrow$

VOID INTERVAL INDICATOR

Δx, DIAL READING

RAW
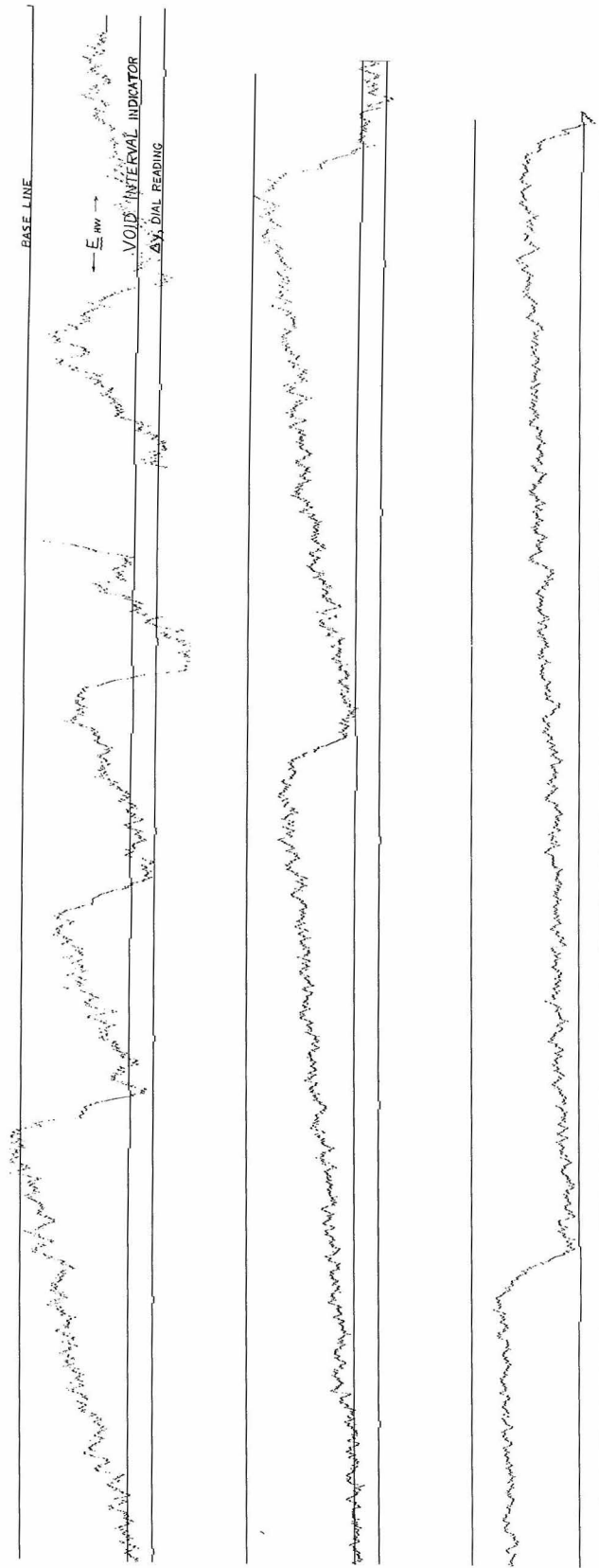
Figure 25. Typical Constant-Current Track. Paper Speed @
3 ft./min. (approx. 1/6 scale)

(a) $y/y_o = 0.991$, with flux

(b) $y/y_o = 0.991$, isothermal

(c) $y/y_o = 0.916$, with same flux as above

(d) $y/y_o = 0.916$, isothermal
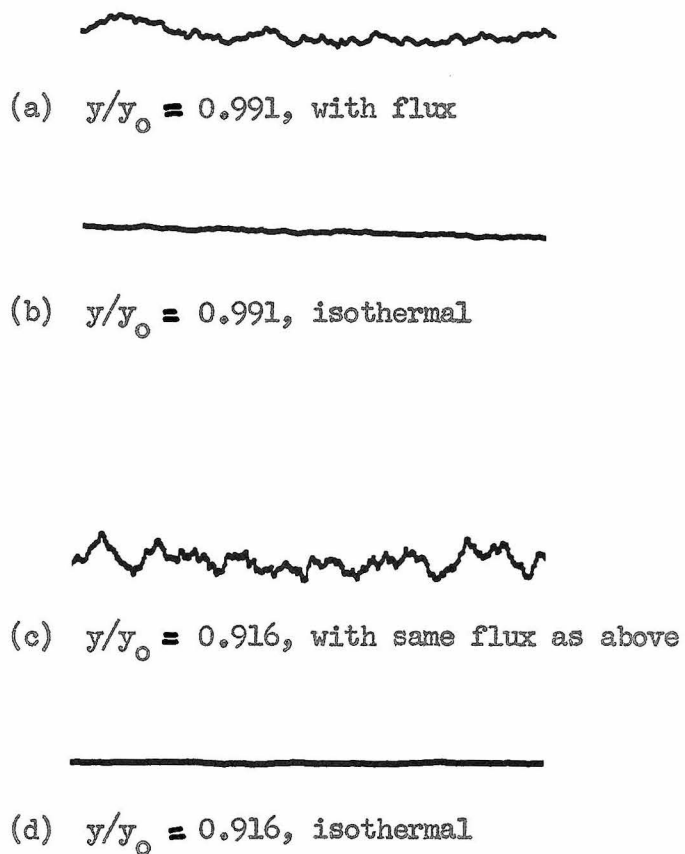
Figure 26.   Deviating Hot-Wire Voltage at Low
Current (10 milliamperes)
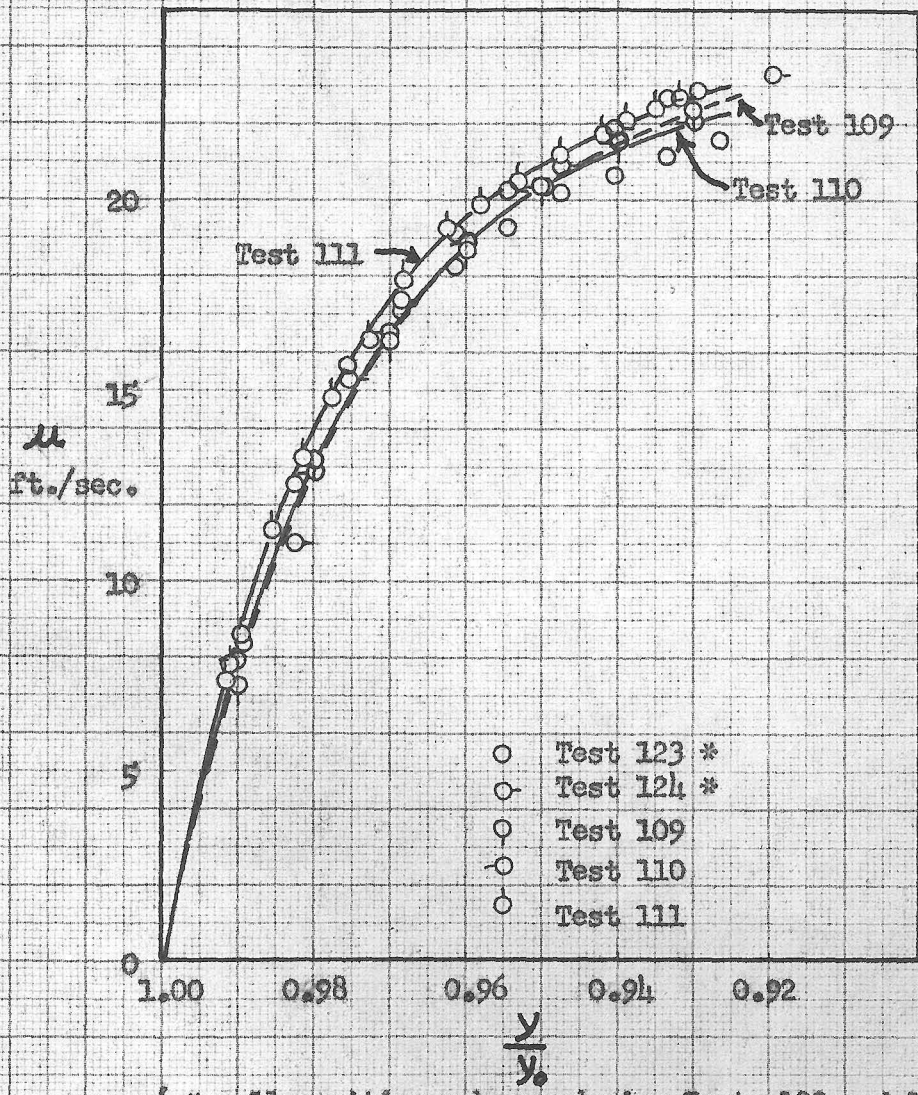
(* wall position unknown during Tests 123 and 124)

Figure 27. Test Velocities
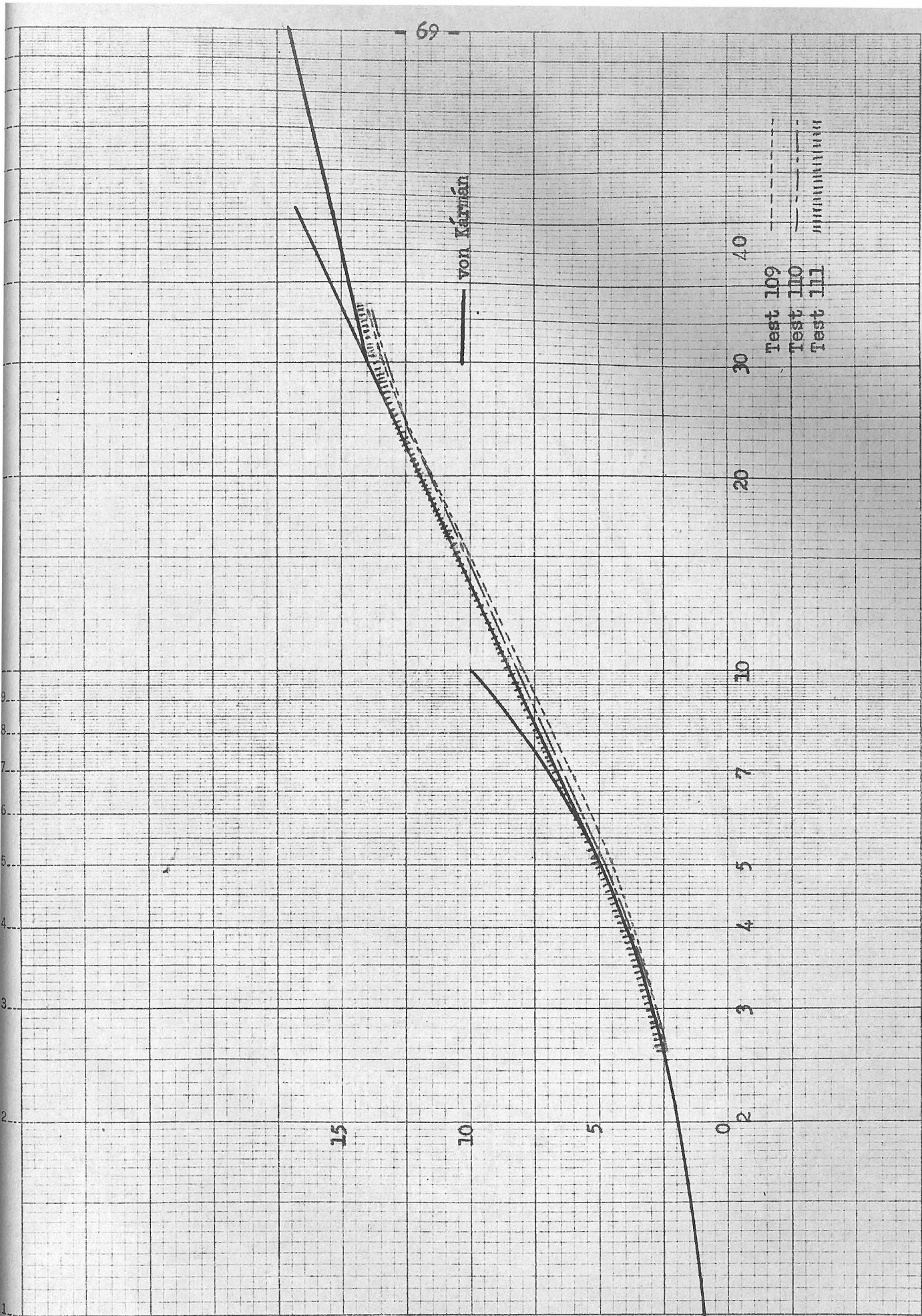
Figure 28. u^+ as a Function of $\log y^+$
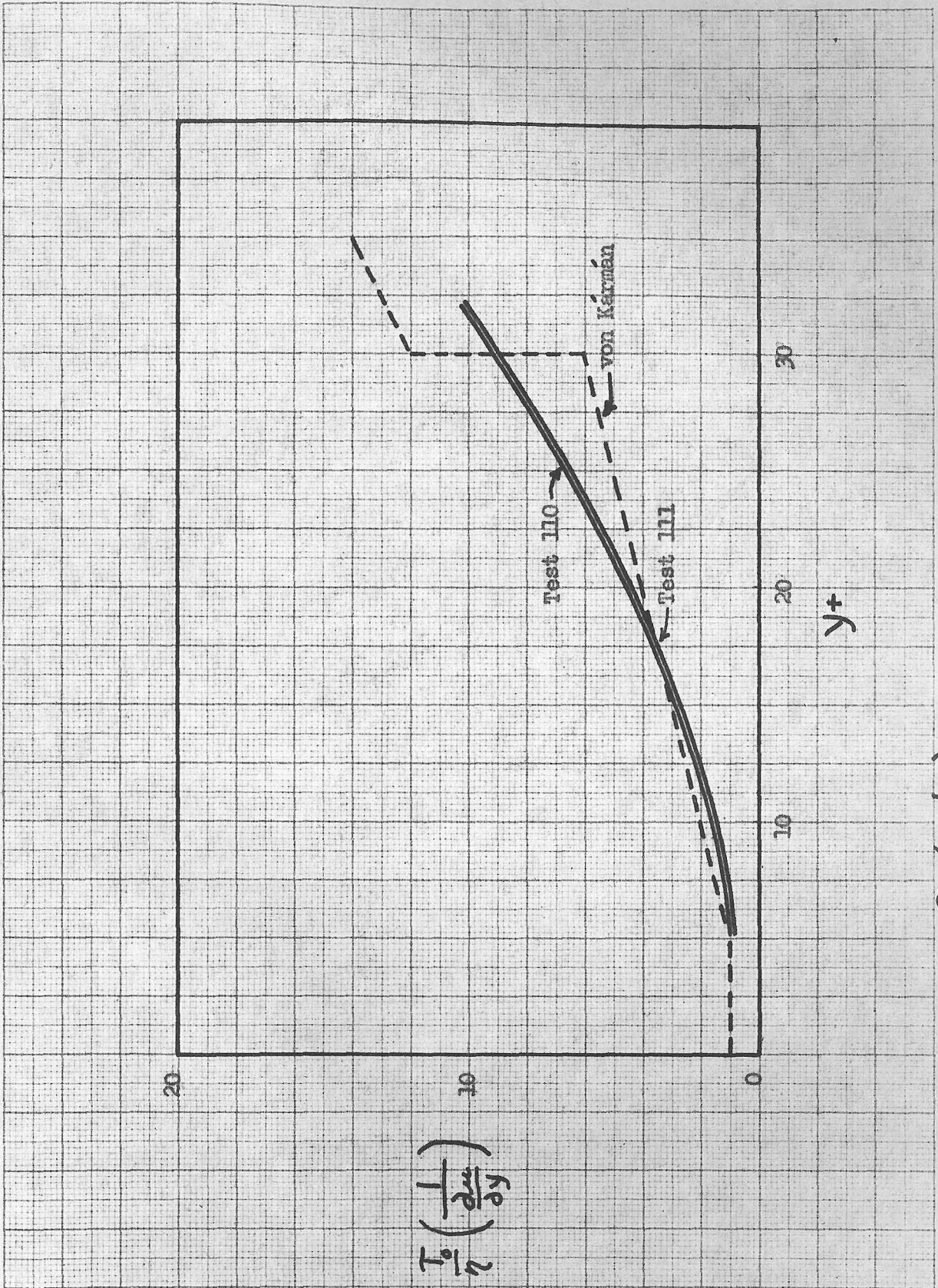
Figure 29. $\frac{\mu}{\tau_0}\left(\frac{du}{dy}\right)$ as a Function of $y+$ for Tests 110 and 111
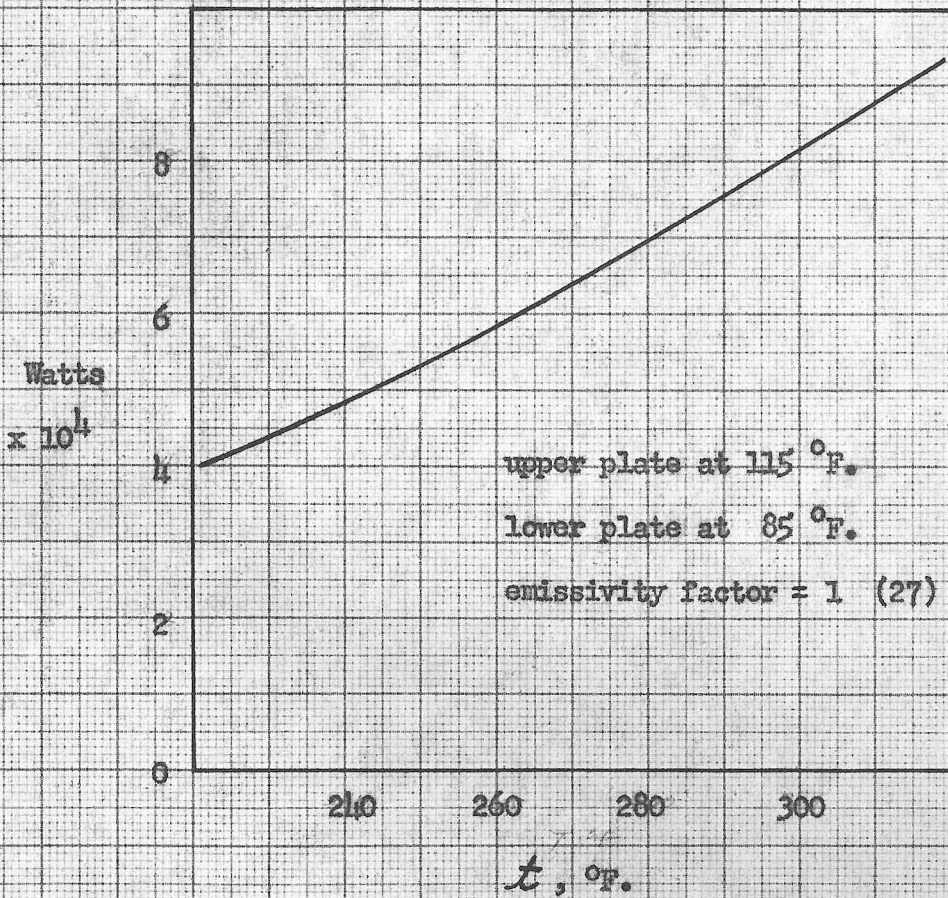
Figure 30. Black Body Radiation Losses from
Hot Wire to Infinite Parallel Plates
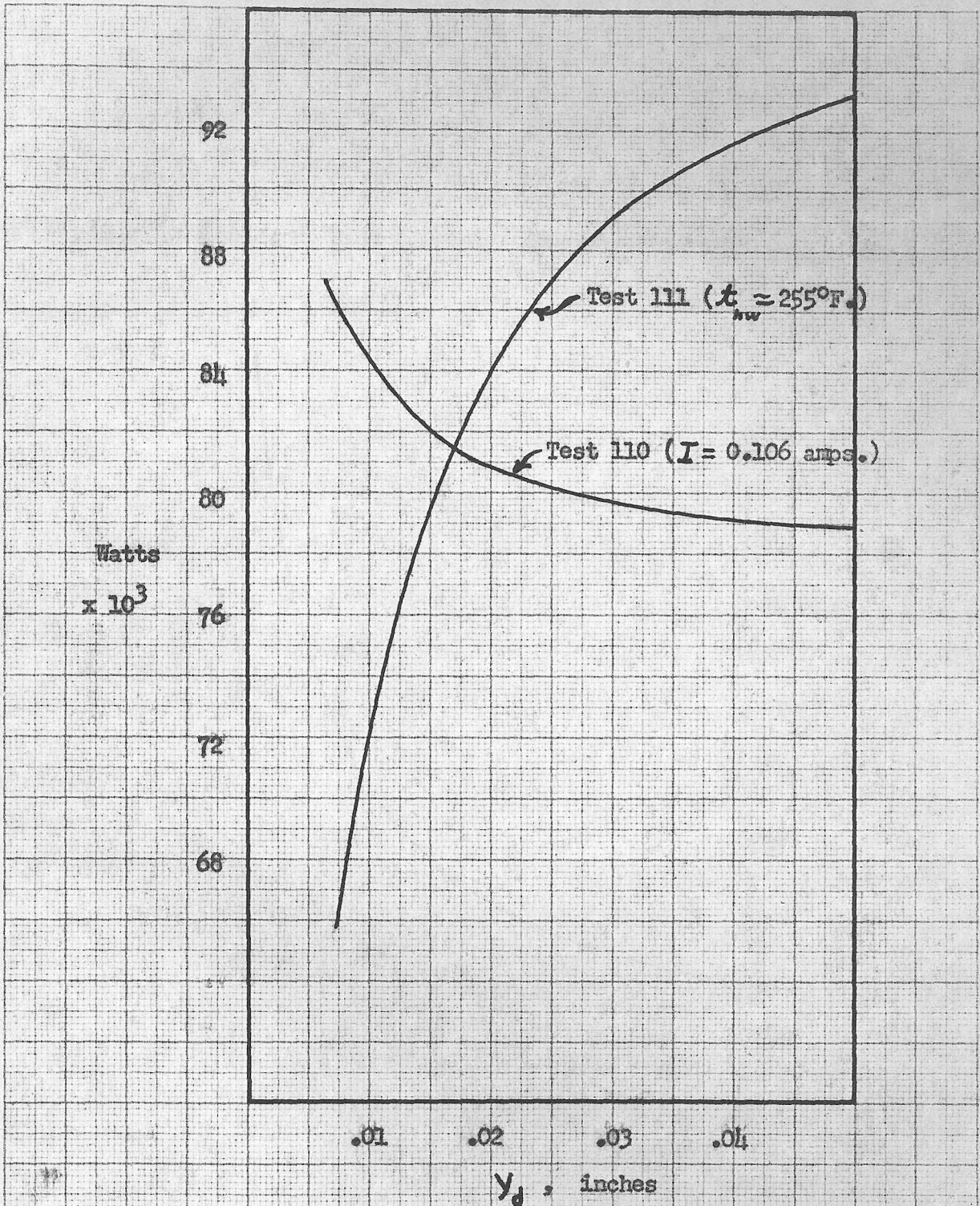
Figure 31. Comparison of Energy Dissipation during Constant-Resistance and Constant-Current Traverses
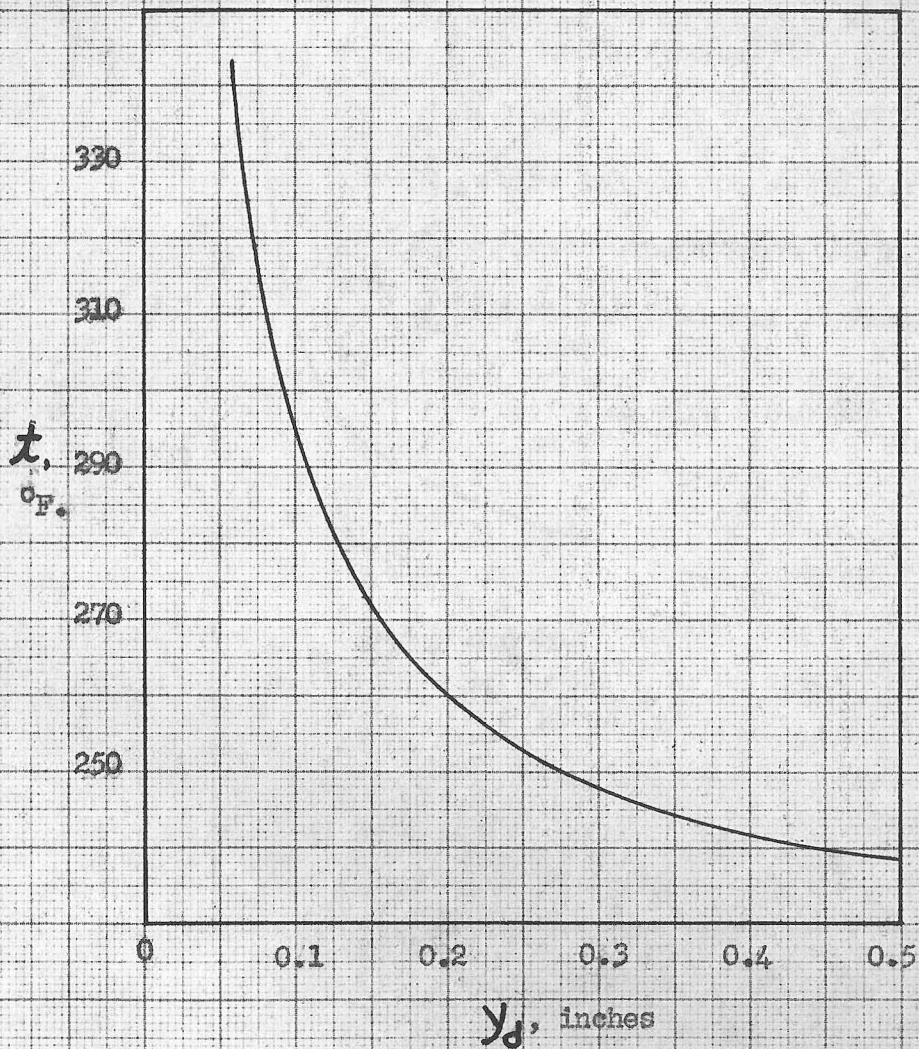
Figure 32. Approximate Wire Temperature during
Constant-Current Test 109
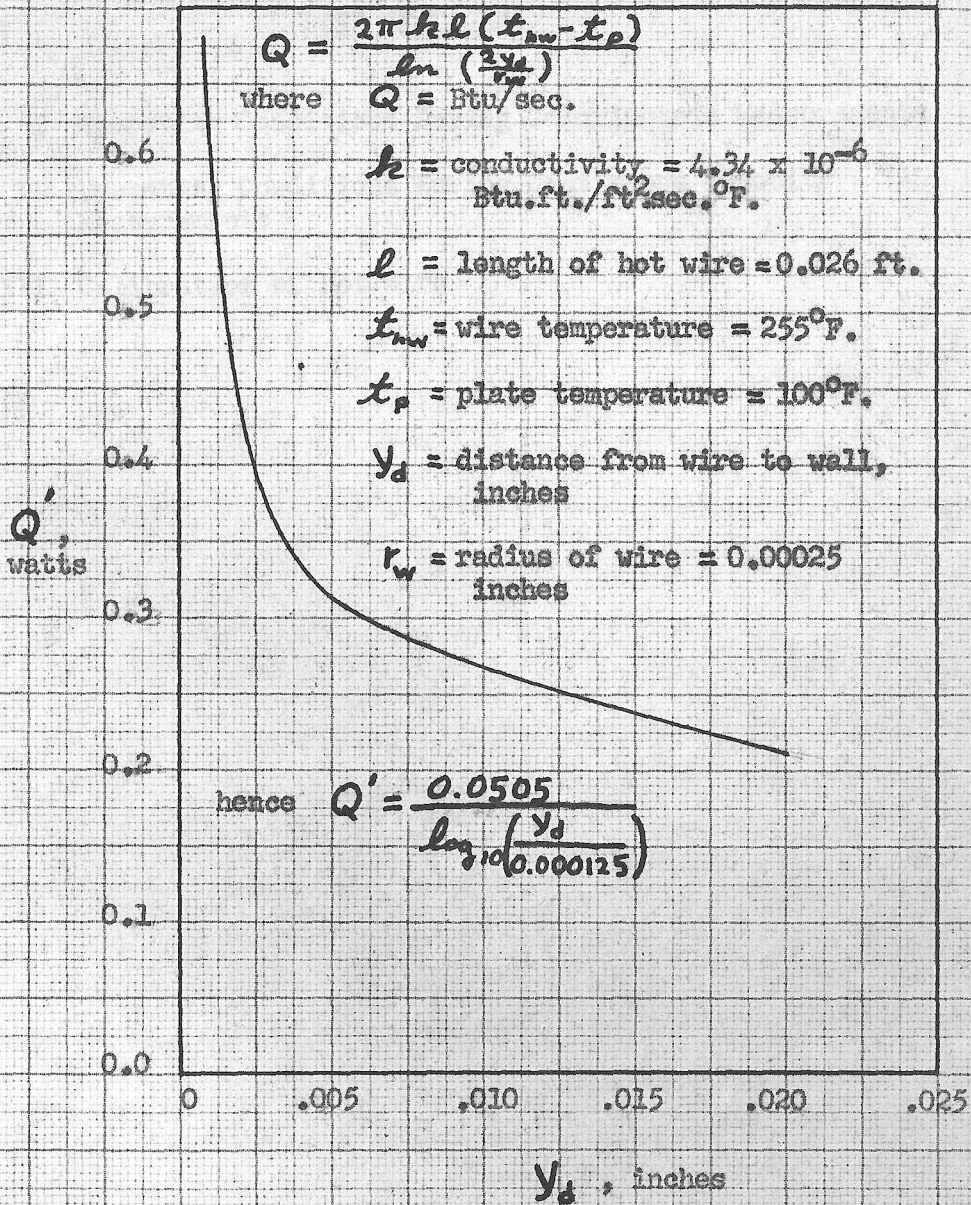
Figure 33. Theoretical Conduction Losses from Wire to Plate

LIST OF TABLES

TABLE I

OPERATING CONDITIONS DURING CALORIMETRIC MEASUREMENTS

Test No.	75		79		81		87	
Calorimeter	1	2	1	2	1	2	1	2
Distance between plates, ft.	0.0575	0.0601	0.0574	0.0599	0.0574	0.0598	0.0576	0.0599
Incoming Air temp., °F.	85.02		100.02		99.96		99.96	
Upper plate temp., °F.	100.06	100.08	114.59	114.60	129.16	129.21	130.14	130.16
Lower plate temp., °F.	71.02	70.82	85.53	85.30	71.10	70.60	70.23	69.48
Reynolds number, x 10^{-4}	1.890		1.852		1.836		3.60	
Composition(wt.fract.H_2O)	0.011		0.011		0.011		0.009	
Channel pressure*, lbs/in^2	14.311		14.348		14.356		14.438	
Barom. pressure, lbs/in^2	14.303		14.339		14.347		14.421	
Gross flux, Btu/ft^{2}sec, x 10^4	226.6	228.3	230.9	231.9	462.2	454.8	785.6	772.3
Room loss corr., Btu/ft^{2}sec, x 10^4	-3.7	-1.7	-8.6	-3.8	-13.6	-6.1	-14.4	-6.4
Plate-Block diff. corr., Btu/ft^{2}sec, x 10^4	0.4	0.5	0.9	0	-2.7	0.7	0	0.2
Isothermal run corr., Btu/ft^{2}sec, x 10^4	-2.3	-2.2	-2.4	-2.6	-5.6	-4.8	-6.7	-7.5
Jacket gradient corr., Btu/ft^{2}sec, x 10^4							1.2	
Net flux, Btu/ft^{2}sec x 10^4	221.0	224.9	220.8	225.5	440.3	444.6	765.7	758.6
Nusselt number	41.28	43.56	40.21	42.50	40.13	41.83	67.74	69.04

TABLE I (Cont.)

Test No.	89		91		94	
Calorimeter	1	2	1	2	1	2
Distance between plates, ft.	0.0576	0.0599	0.0576	0.0599	0.0576	0.0599
Incoming Air temp., °F.	100.03		99.95		99.98	
Upper plate temp., °F.	129.99	130.03	129.96	129.99	115.01	115.02
Lower plate temp., °F.	70.42	69.54	70.23	69.76	85.11	84.87
Reynolds number, x 10^{-4}	5.58		0.975		3.88	
Composition(wt.fract.H_2O)	0.012		0.009		0.008	
Channel pressure*, lbs/in²	14.261		14.278		14.389	
Barom. pressure, lbs/in²	14.231		14.276		14.372	
Gross flux, Btu/ft²sec, x 10^4	1087.2	1067.5	280.7	266.2	414.8	406.6
Room loss corr., Btu/ft²sec, x 10^4	-14.6	-6.5	-14.6	-6.6	-9.4	-4.2
Plate-Block diff. corr., Btu/ft²sec, x 10^4	-2.9	0	-0.9	0	0	-0.7
Isothermal run corr., Btu/ft²sec, x 10^4	-21.2	-19.3	-9.0	-7.3	-6.3	-7.0
Jacket gradient corr., Btu/ft²sec, x 10^4	5.5				0.8	
Net flux, Btu/ft²sec, x 10^4	1054.0	1041.7	256.3	252.3	399.9	394.7
Nusselt number	93.90	94.97	22.77	23.10	70.88	72.29

* Measured 3 inches downstream from the center of the downstream calorimeter (#2)

TABLE II

OPERATING CONDITIONS DURING CONTINUOUS VELOCITY MEASUREMENTS

Test No.	123	124	109	110	111
Method	Const.Res.	Const.Res.	Const.Curr.	Const.Curr.	Const.Res.
Distance between plates at center of channel, ft.	.060	.060	.060	.0600	.0603
Incoming Air Temp., °F.	100	100	100.17	100.07	100.21
Upper Plate Temp., °F.	114	114	114.44	100.01	100.18
Lower Plate Temp., °F.	86	86	85.79	100.07	100.00
Max. velocity, ft./sec.	29.29	30.54	30.53	30.47	30.45
Reynolds Number, x 10^{-4}*	1.70	1.70	1.692	1.697	1.702

* From Figure 6

TABLE III

CALIBRATION OF HOT WIRE

Test	123	124	109	110 before	110 after	111 before	111 after
R_{hw}	7.259	7.269	-	-	-	7.264	7.273
I	-	-	-	0.0955	0.0955	-	-
$\mu_1^{\frac{1}{2}}$	5.41	5.53	5.53	5.52	5.52	5.52	5.51
Φ_1	0.0584	0.0634	0.0610	0.0606	0.0604	0.0639	0.0639
$\mu_2^{-\frac{1}{2}}$	-	4.26	4.22	4.28	4.25	4.26	4.27
Φ_2	-	0.0530	0.0520	0.0517	0.0516	0.0533	0.0532
μ_3	3.44	3.47	3.40	3.51	3.49	3.44	3.44
$\Phi_3^{-\frac{1}{2}}$	0.0440	0.0467	0.0449	0.0459	0.0459	0.0459	0.0458
μ_4	2.36	2.57	2.77	2.81	2.85	2.77	2.77
Φ_4	0.0360	0.0378	0.0406	0.0404	0.0389	0.0397	0.0396